Article

Cell

Sour Sensing from the Tongue to the Brain

Graphical Abstract

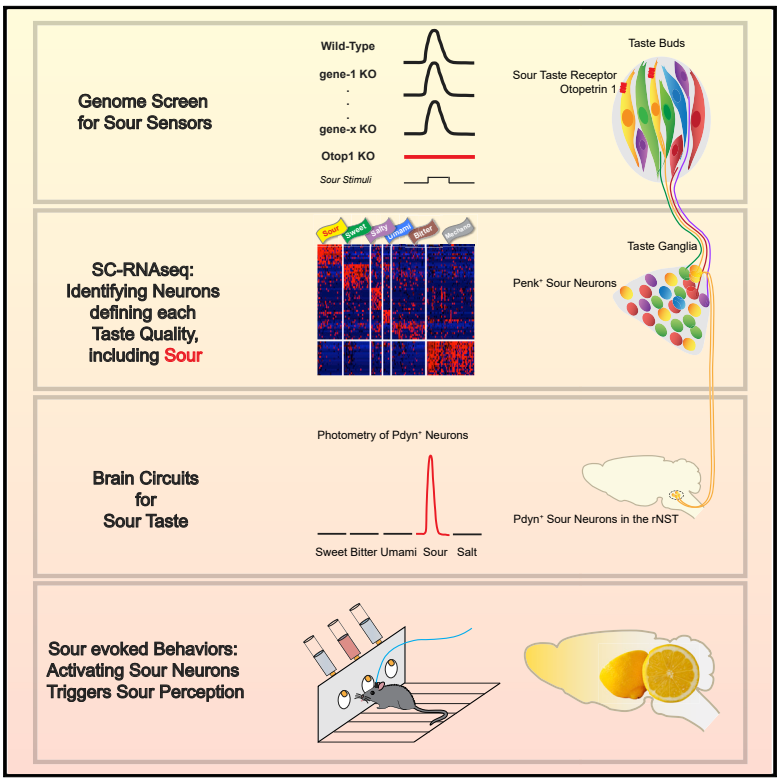

Highlights

- OTOP1 is the mammalian sour taste receptor
- Expression of OTOP1 in sweet taste cells allows them to respond to sour stimuli
- Neurons mediating the five basic tastes (sweet, bitter, salty, umami, and sour) are genetically distinct from each other
- The circuit mediating responses to sour is hardwired to evoke behavioral aversion to acid stimuli

Authors

Jin Zhang, Hao Jin, Wenyi Zhang, Cheng Ding, Sean O'Keeffe, Mingyu Ye, Charles S. Zuker

Correspondence

cz2195@columbia.edu

In Brief

The detection of sour is mediated by the Otop1 proton channel present in sour-sensing taste receptor cells. These taste cells are selectively wired to dedicated neurons and brain circuits triggering innately aversive reactions to acid stimuli.

Zhang et al., 2019, Cell *179*, 1–11
October 3, 2019
https://doi.org/10.1016/j.cell.2019.08.031

CellPress

Please cite this article in press as: Zhang et al., Sour Sensing from the Tongue to the Brain, Cell (2019), https://doi.org/10.1016/j.cell.2019.08.031

Article

Cell

Sour Sensing from the Tongue to the Brain

Jin Zhang,[1,2,3,4,5] Hao Jin,[1,2,3,4,5] Wenyi Zhang,[1,2,3,4] Cheng Ding,[1,2,3,4] Sean O'Keeffe,[2,6] Mingyu Ye,[1,2,3,4] and Charles S. Zuker[1,2,3,4,7,*]

[1]Howard Hughes Medical Institute, Columbia University, New York, NY 10032, USA
[2]Department of Biochemistry and Molecular Biophysics, Columbia University, New York, NY 10032, USA
[3]Department of Neuroscience, Columbia University, New York, NY 10032, USA
[4]Mortimer B. Zukerman Mind Brain and Behavior Institute, Columbia University, New York, NY 10027, USA
[5]These authors contributed equally
[6]Present address: Regeneron Pharmaceuticals, Inc. Tarrytown, NY 10591, USA
[7]Lead Contact
*Correspondence: cz2195@columbia.edu
https://doi.org/10.1016/j.cell.2019.08.031

SUMMARY

The ability to sense sour provides an important sensory signal to prevent the ingestion of unripe, spoiled, or fermented foods. Taste and somatosensory receptors in the oral cavity trigger aversive behaviors in response to acid stimuli. Here, we show that the ion channel Otopetrin-1, a proton-selective channel normally involved in the sensation of gravity in the vestibular system, is essential for sour sensing in the taste system. We demonstrate that knockout of Otop1 eliminates acid responses from sour-sensing taste receptor cells (TRCs). In addition, we show that mice engineered to express otopetrin-1 in sweet TRCs have sweet cells that also respond to sour stimuli. Next, we genetically identified the taste ganglion neurons mediating each of the five basic taste qualities and demonstrate that sour taste uses its own dedicated labeled line from TRCs in the tongue to finely tuned taste neurons in the brain to trigger aversive behaviors.

INTRODUCTION

Among the five basic taste qualities (sweet, bitter, umami, salty, and sour), acid or sour sensing is particularly unique because it is mediated not only by the taste system (Huang et al., 2006) but also by the somatosensory system via Trpv1-expressing neurons innervating the oral cavity (Caterina et al., 1997; Julius, 2013; Leffler et al., 2006). Acid detection triggers innately aversive responses, ensuring that acidic stimuli, often noxious and dangerous to animals, are rejected while also guaranteeing that unripe, spoiled, or fermented foods are not ingested (Yarmolinsky et al., 2009).

The taste receptor cells (TRCs) responsible for sour taste were identified over a decade ago using a combination of molecular, electrophysiological, and cell ablation studies (Huang et al., 2006). Sour TRCs are unique and distinct from the TRCs mediating each of the other four basic taste qualities and are defined by expression of the polycystin-2-like 1 (Pkd2l1) gene (Huang et al., 2006). Notably, although genetic ablation of the Pkd2l1-expressing TRCs completely abolished sour taste responses (Huang et al., 2006), mice lacking the actual Pkd2l1 gene and/or its associated partner Pkd1l3 still exhibited robust sour-evoked taste responses (Horio et al., 2011; Nelson et al., 2010).

Many genes expressed in sour-sensing cells have been proposed to function as the acid-sensing receptor, including acid-sensitive ion channels (ASICs) (Lin et al., 2002; Ugawa et al., 1998, 2003), hyperpolarization-activated cyclic nucleotide-gated channels (HCNs) (Stevens et al., 2001), potassium two-pore domain channel subfamily K (KCNK) (Lin et al., 2004; Richter et al., 2004), and the inward rectifier potassium ion channel $K_{IR}2.1$ (Challis and Ma, 2016; Ye et al., 2016). Most recently, elegant studies by Tu et al. (2018) identified Otopetrins, a family of proton-conducting ion channels first recognized in the vestibular system and thought to be involved in spatial orientation and acceleration (Hughes et al., 2004, 2007, 2008), as sour receptor candidates.

Here, we demonstrate that Otopetrin-1 is required by sour-sensing taste cells *in vivo* to respond to acid stimuli and functions as the sour taste receptor. Next, we used single-cell RNA sequencing (RNA-seq) in combination with genetic and behavioral studies to identify the ganglion neurons mediating each of the five basic taste qualities. We demonstrate that signals from sour-sensing taste cells in the tongue are transmitted to and represented in the brain by a genetically defined population of sour-responding neurons hardwired to trigger aversive behaviors.

RESULTS

Otop1 Knockout Animals Lack Sour Taste Responses

To identify candidate sour taste receptors, we molecularly characterized the repertoire of genes expressed in sour (Pkd2l1-expressing) taste cells using a combination of bulk and single-cell RNA sequencing (scRNA-seq). We performed scRNA-seq on over 400 sour TRCs isolated from animals expressing the tdTomato reporter in Pkd2l1-expressing taste cells (Huang et al., 2006) and also carried out bulk RNA-seq from hundreds of "non-sour" TRCs and surrounding tongue epithelia (see STAR Methods for details) to search for genes preferentially expressed in sour versus other classes of cells in the tongue. Overall, we classified 115 genes encoding putative transmembrane

Please cite this article in press as: Zhang et al., Sour Sensing from the Tongue to the Brain, Cell (2019), https://doi.org/10.1016/j.cell.2019.08.031

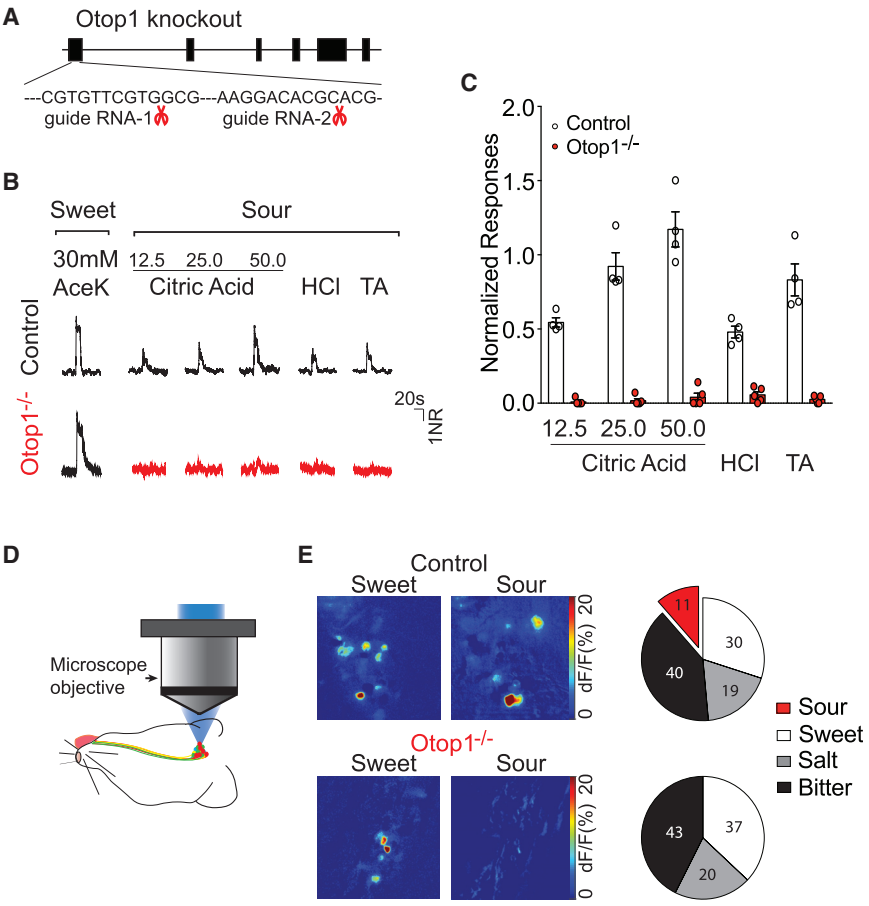

Figure 1. Otop1 Knockout Animals

(A) Schematic drawing illustrating the structure of the murine Otop1 gene and the strategy for generating knockouts using CRISPR-Cas9. Partial sequences of the two guide RNAs are shown below exon 1; red scissors denote the cutting positions. See Figure S2 for immunostaining of Otop1 in TRCs from WT versus Otop1$^{-/-}$ animals.

(B) WT animals (control) showed robust *chorda tympani* nerve responses to a wide range of sour tastants, including citric acid (12.5 mM, 25 mM, and 50 mM), hydrochloric acid (HCl; 10 mM), and tartaric acid (TA; 50 mM); also shown are sweet taste responses (30 mM acesulfame K [AceK]). In contrast, Otop1 knockout animals (Otop1$^{-/-}$) exhibited a major loss of responses to sour stimuli. However, responses to sweet (30 mM AceK, bottom panel) and other taste qualities remained unimpaired (Figure S1C). Note that, to block residual responses to acid from bitter T2Rs (Oka et al., 2013), the nerve recordings were carried out in the presence of the bitter TRC blocker allyl isothiocyanate (AITC) (Barretto et al., 2015; Oka et al., 2013); see Figure S1C for details. NR, normalized response to 30 mM AceK; see STAR Methods.

(C) Quantification of nerve responses of WT control (white) and Otop1$^{-/-}$ (red) animals. Nerve responses to sour stimuli were normalized to the responses to 30 mM AceK. Multiple unpaired t tests, all acid stimuli, $p < 0.001$. Values are means ± SEM. WT, n = 4; Otop1$^{-/-}$, n = 5 (the average of 2 separate recording sessions was used for each animal).

(D) Diagram illustrating optical access to the geniculate ganglion (see also Barretto et al., 2015).

(E) Calcium responses in control (top panels) and Otop1$^{-/-}$ animals (bottom panels). The left panels show the geniculate ganglion with neurons responding to sweet stimuli (AceK, 30 mM), and the right panel depicts the same field after sour stimulation (citric acid, 50 mM). The two bottom panels show responses in the Otop1$^{-/-}$ mutants. Note that responses from sour cells are absent. Scale, ΔF/F. The pie charts indicate the percentage of geniculate neurons responding to each individual taste stimulus in control (Barretto et al., 2015; Lee et al., 2017) and Otop1$^{-/-}$ mutants. WT (n = 7 mice), 78 neurons imaged; Otop1$^{-/-}$ knockout animals (n = 7 mice), 92 neurons imaged; none were tuned to sour. Tastants: sour, 50 mM citric acid; sweet, 30 mM AceK; salty, 60 mM NaCl; bitter, 1 mM cycloheximide.

proteins as enriched in sour TRCs (Table S1) and selected 7 candidate membrane receptors and ion channels for genetic knockout.

To determine the effect of a loss-of-function mutation in sour receptor candidate genes, we examined homozygous knockout and control animals using a two-stage strategy. First, we recorded tastant-evoked responses from one of the principal nerves innervating TRCs in the tongue; this physiological assay monitors the activity of the taste system at the periphery and provides a reliable measure of TRC function (Dahl et al., 1997; Nelson et al., 2002). Then we performed *in vivo* functional calcium imaging and recorded the responses of taste ganglion neurons to stimulation of the tongue with tastants representing all taste qualities. We anticipated that, if a candidate were essential for sour taste, then knocking out the gene should abolish most, if not all, responses to acid stimuli in both assays.

We generated and tested homozygous knockout animals for Slc38a5, Slc38a11, Kcnk1, Kcnk16, and Hcn3 (Figure S1); we also obtained and tested homozygous knockout animals for Trpm2 (Yamamoto et al., 2008). None of these mutants had significant deficits in their responses to sour stimuli (Figure S1). Next, we generated animals with a homozygous deletion of Otopetrin-1 (Otop1$^{-/-}$; Figures 1A and S2), the last candidate identified in our screen, also recently proposed by Tu et al. (2018) to function as a candidate sour receptor. Our results demonstrated that Otop1$^{-/-}$ mice had a dramatic loss of sour taste; nerve responses to a wide range of sour stimuli, including strong and weak acids, were largely abolished (Figures 1B, 1C, and S1), even at concentrations tens of times higher than those required to trigger strong responses in wild-type (WT) mice (Huang et al., 2006). Importantly, responses to other taste qualities were unaffected (Figure S1).

Next, we examined the taste responses of Otop1$^{-/-}$ mice using functional imaging. We targeted the genetically encoded calcium indicator GCaMP6s (Chen et al., 2013) to taste ganglion neurons using retrograde viral transduction from their projections in the nucleus of the solitary tract (NST) (Barretto et al., 2015), exposed a small imaging window allowing optical access to the entire ganglion *in vivo*, and recorded tastant-evoked responses (Figure 1D). As expected, when we examined taste

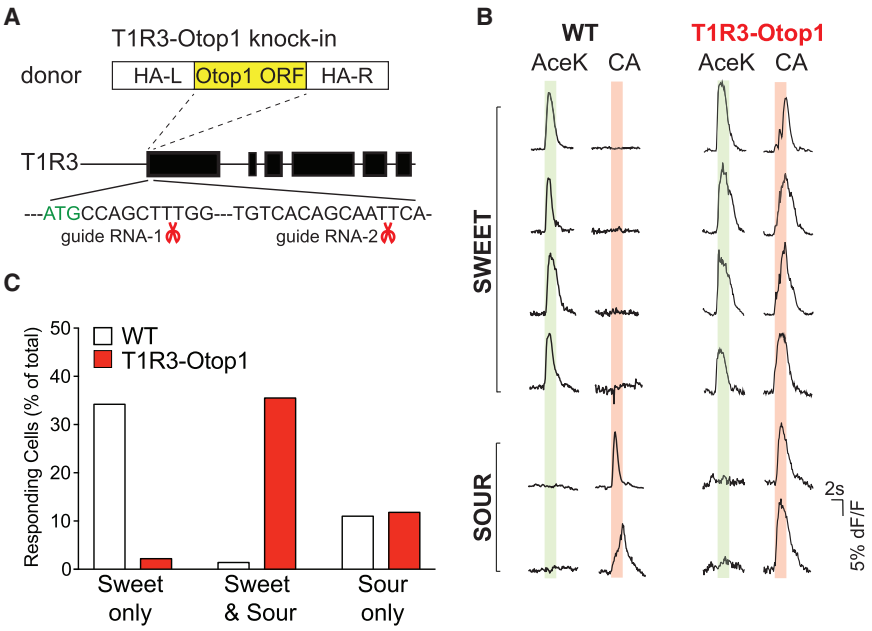

Figure 2. Endowing Sweet Cells with Responses to Sour Stimuli: T1R3-Otop1

(A) Schematic drawing illustrating the structure of the murine Tas1r3 gene (T1R3) (Nelson et al., 2001) and the strategy for generating the T1R3-Otop1 knockin animals using CRISPR-Cas9. The donor vector, including the left and right homology arms (HA-L, 2 kb; HA-R, 2 kb) and the murine Otop1 open reading frame (ORF) are shown on top of the T1R3 gene diagram. The start codon (green) and partial sequences of the two guide RNAs are shown below exon 1; red scissors denote the cutting positions. See also Figure S2.

(B) Calcium responses from individual taste ganglion neurons of WT (left panel) and T1R3-Otop1 heterozygous knockin animals (right panel) following sweet (30 mM AceK) and sour (50 mM citric acid) stimuli. Shown are recordings from 6 sample neurons; the green- and red-shaded bars indicate the duration of the stimulus (2 s). Scale, ΔF/F. In contrast to WT controls, sweet neurons respond robustly to sour stimuli in T1R3-Otop1 knockin animals, whereas their sour responses remained unaffected. Other taste qualities were also normal in T1R3-Otop1 animals (data not shown).

(C) Percentage of geniculate neurons responding to sweet and sour taste stimuli in control (open bars) and T1R3-Otop1 knockin animals (red bars). Neurons were examined for their tuning to various tastes without pre-selection. Note that nearly all neurons that responded to sweet in T1R3-Otop1 mice also responded to sour stimuli. The distribution in control animals matches reported data (Barretto et al., 2015; Lee et al., 2017). WT (n = 4 mice), 73 neurons imaged; 24 responded to sweet alone, and 8 responded to sour alone. T1R3-Otop1 mis-expression animals (n = 4 mice), 93 neurons imaged; only 3 responded to sweet alone, but 36 responded to both sweet and sour stimuli. The expected fraction responded to sour alone (11 neurons) (Barretto et al., 2015).

responses from control animals, different geniculate ganglion neurons responded robustly to individual taste qualities (sweet neurons, bitter neurons, sour neurons, etc.; Figure 1E, top panels; Barretto et al., 2015; Lee et al., 2017), and the representation of each taste quality in the ganglia recapitulated the previously reported distributions (e.g., ~40% of the neurons respond to bitter, ~30% to sweet, ~10% to sour, and ~20% to salt) (Barretto et al., 2015; Lee et al., 2017). In sharp contrast, Otop1$^{-/-}$ mutant animals lacked acid responses in sour ganglion neurons (Figure 1E, bottom panels). Together, these results substantiate the Otopetrin-1 proton-selective ion channel as essential for acid-evoked responses in sour TRCs and as a strong candidate for being the sour taste receptor.

Targeted Expression of Otop1 in Sweet TRCs

We predicted that, if OTOP1 functions as the sour taste receptor, then ectopic expression should endow the recipient cells with sensitivity to acid stimuli. Thus, we engineered mice where we knocked the Otop1 gene into the sweet receptor T1R3 locus (T1R3-Otop1; Figures 2A and S2) for targeted expression in sweet TRCs. In essence, we used the CRISPR-Cas9 system to introduce the entire OTOP1 ion channel protein-coding DNA fragment downstream of the T1R3 ATG initiator codon, thus directing expression of OTOP1 under T1R3 gene control (STAR Methods). We then examined the tuning properties of the sweet TRCs by *in vivo* functional calcium imaging experiments (Figure 1D). Because the taste selectivity of ganglion neurons reflects the identity of the TRCs to which they connect, we compared the responses of sweet ganglion neurons to stimulation of the tongue with sweet versus sour stimuli in control and the engineered T1R3-Otop1 animals. As anticipated, sweet TRCs from control animals respond robustly to sweet but not sour stimuli (Figure 2B, left panel). In sharp contrast, sweet neurons of TR1R3-Otop1 knockin mice respond not only to sweet tastants but, in addition, were also activated by sour stimuli (Figure 2B, right panel). Indeed, we recorded sweet neurons from multiple TR1R3-Otop1 animals, and over 95% of the sweet neurons also responded to sour stimuli (Figure 2C). Taken together, these Otop1 gain-of-function and loss-of-function experiments prove OTOP1 as the sour taste receptor.

Transcriptionally Defined Populations in the Taste Ganglia

Previously we showed that the different taste qualities are mediated by dedicated TRCs tuned to individual tastes and innervated by dedicated ganglion neurons tuned to matching taste qualities (Barretto et al., 2015; Lee et al., 2017). This one-taste one-TRC "labeled line" is a hallmark of the taste system and the basis of taste coding at the periphery, but how is the sour taste information detected and transmitted from the tongue represented in the brain? We reasoned that this question can be answered by genetically marking the sour-responding ganglion neurons and identifying their targets in the brain.

We performed single-cell RNA-seq on 800 neurons from the geniculate ganglion, pre-selected by their expression of P2rx3, a receptor for the neurotransmitter mediating TRC-to-ganglion synaptic transmission (Huang et al., 2011). From this set, we classified 454 neurons as expressing Phox2b (see Figure S3), a marker for sensory neurons (D'Autréaux et al., 2011), and performed t-Distributed Stochastic Neighboring Embedding

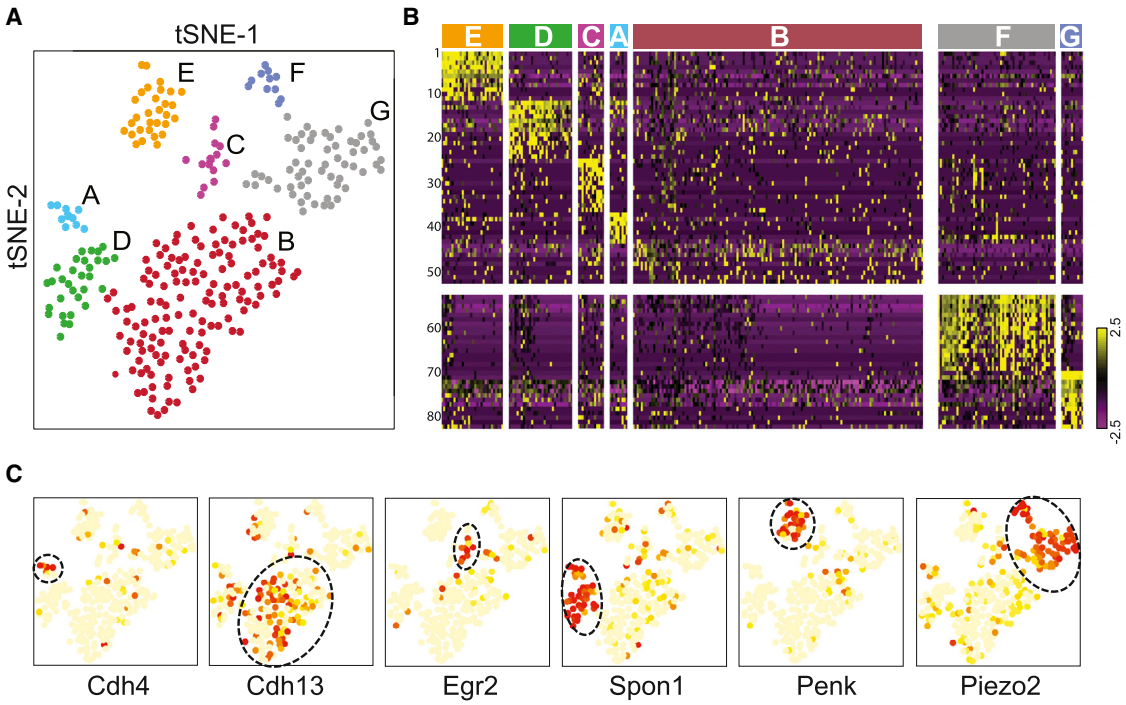

Figure 3. Different Classes of Taste Neurons in Taste Ganglia

(A) Two-dimensional t-distributed stochastic neighbor embedding (tSNE) plot.

(B) Heatmap illustrating expression of 82 selected gene markers in clusters A–G (Table S2). Individual clusters are separated by white lines; candidate gustatory neurons: A–E; somatosensory (expressing Piezo2): F–G. Expression levels are pseudocolored based on *Z* scores from −2.5 (purple) to 2.5 (yellow).

(C) Sample transcriptional markers defining each cluster. Cluster A, Cdh4 ($p = 1.15 \times 10^{-5}$); cluster B, Cdh13 ($p = 6.36 \times 10^{-8}$), cluster C, Egr2 ($p = 1.06 \times 10^{-9}$); cluster D, Spon1 ($p < 1 \times 10^{-15}$); cluster E, Penk ($p < 1 \times 10^{-15}$). Piezo2 marks clusters F and G. Violin plots for these markers are shown in Figure S3. Ten colors in the yellow-to-red spectrum represent every 10^{th} percentile; light yellow, lowest 10% in expression; red, highest 10%.

(tSNE) analysis to identify and visualize their distribution into different neuronal groups. Our results (Figures 3A and 3B) revealed 5 distinct clusters (labeled A–E), each potentially defining one of the five basic taste qualities. As anticipated, we also identified 2 putative somatosensory clusters (labeled F and G), characterized by high levels of expression of the mechanosensory channel Piezo2 (Figures 3C and S3; Coste et al., 2010; Ranade et al., 2014; Xiao and Xu, 2010). A previous effort to characterize genetically defined geniculate taste neurons analyzed small numbers of cells and, therefore, did not have enough single-cell RNA-seq data to resolve multiple candidate taste classes (Dvoryanchikov et al., 2017).

Neurons for Each Taste: Penk Marks a Distinct Sour-Sensing Population in the Geniculate Ganglion

To identify the sour-sensing population, we set up a screening strategy based on a combination of genetic knockouts, neuronal ablation, or functional imaging to characterize neurons in each of the five Phox2b-positive clusters (Figure 3B; Table S2).

First we tested clusters A and B, marked by selective expression of cadherin Cdh4 and Cdh13, respectively (Figures 3C and S3). The cadherin family is a major class of cell surface recognition molecules with important roles in neuronal wiring and synaptic specificity (Basu et al., 2015; Sanes and Yamagata, 2009; Yogev and Shen, 2014). We hypothesized that, if cadherins are essential for the proper connectivity of specific subsets of geniculate ganglion neurons (see, for example, Lee et al., 2017), then knocking out Cdh4 and Cdh13 may expose selective deficits in taste. Indeed, animals carrying a homozygous deletion of Cdh4 ($Cdh4^{-/-}$; Dickinson et al., 2016) are no longer attracted to umami tastants (Figures 4A and 4B), whereas animals carrying a homozygous deletion of Cdh13 (Poliak et al., 2016) exhibited a dramatic impairment in bitter taste aversion (Figure 4C). Importantly, in both cases, responses to other taste stimuli were unaffected (Figure S4). To examine cluster C, marked by expression of Egr2 (Figures 3C and S3), we genetically silenced synaptic activity in neurons expressing Egr2-Cre (Voiculescu et al., 2000) by targeting expression of a Cre-dependent tetanus toxin construct. Our results revealed a highly specific deficit in salt taste (Figure 4D), whereas the behavioral responses to other tastants remained unimpaired (Figure S4).

Finally, we assayed the tastant selectivity of the ganglion neurons in clusters D and E by recording their taste-tuning properties. In essence, we targeted expression of the GCaMP6s calcium reporter to cluster D using a Spondin1-Cre driver line and to cluster E using a Penk-Cre driver line, respectively (see Figure 3C and STAR Methods for details regarding engineering of the various driver lines). Our results demonstrated that Spondin1-expressing cells represent sweet taste neurons (Figure 4E), whereas Penk-expressing neurons

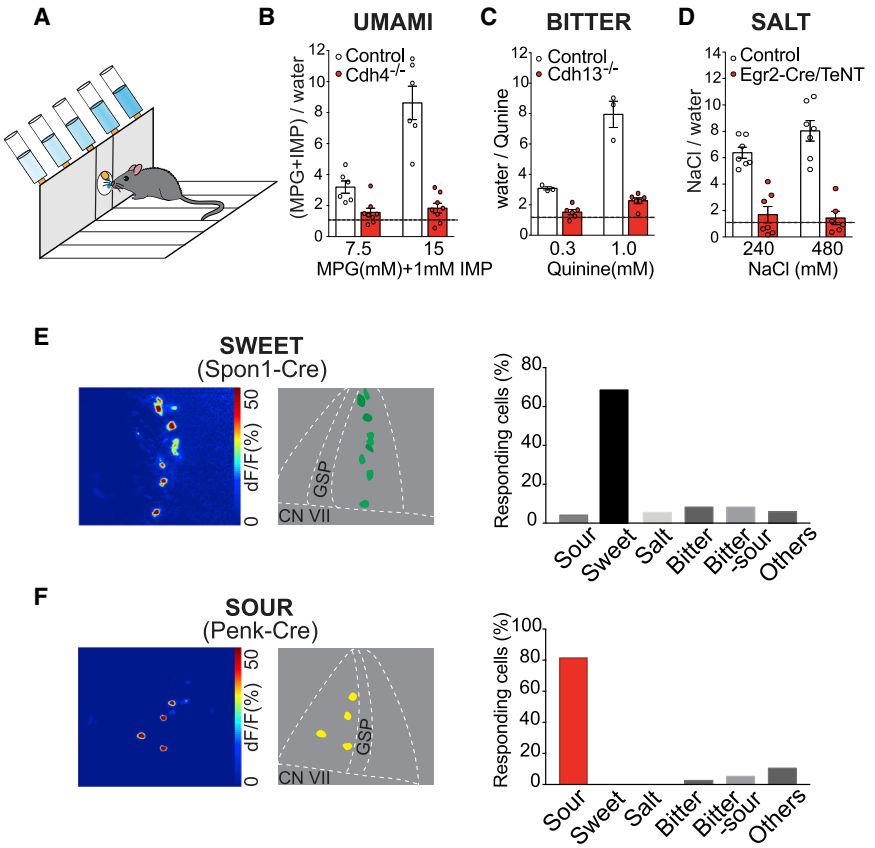

Figure 4. Penk Marks the Sour-Sensing Population in the Geniculate Ganglion

(A) Cartoon illustrating the brief access taste preference assay. Mice were presented with one of various test solutions in each trial, and licks were recorded as a proxy for the animal's preference (Zhang et al., 2003).

(B) Umami preference of control (white bars, n = 6) and Cdh4 homozygous knockout animals ($Cdh4^{-/-}$, red, n = 8) are shown relative to water. $Cdh4^{-/-}$ animals no longer exhibit a preference for umami solutions; shown are responses to 7.5 mM and 15 mM mono-potassium glutamate (MPG) plus 1 mM inosine mono-phosphate (IMP) (Zhao et al., 2003). However, their behavioral responses to other tastes remained unaffected (Figure S4). Values are means ± SEM. Multiple unpaired t tests; 7.5 mM, $p = 0.004$; 15 mM, $p < 0.001$.

(C) Bitter aversion of control (white bars, n = 3) and Cdh13 homozygous knockout animals ($Cdh13^{-/-}$, red, n = 6). $Cdh13^{-/-}$ animals have a profound loss of aversion to bitter solutions (quinine, 0.3 and 1 mM). However, their behavior to other tastes was unaffected (Figure S4). Values are means ± SEM. Multiple unpaired t tests; 0.3 mM, $p = 0.009$; 1 mM, $p = 0.003$.

(D) Salt preference of WT mice (control, white, n = 7) and animals with Egr2-expressing neurons silenced by targeted expression of tetanus toxin (Zhang et al., 2008) (red, n = 7). Both groups were salt-deprived before the behavioral test (STAR Methods; Chandrashekar et al., 2010). Egr2-TeNT animals exhibited a dramatic loss of salt attraction (NaCl, 240 and 480 mM), whereas their behavioral responses to other tastes remained unaffected (Figure S4). Values are means ± SEM. Multiple unpaired t tests, $p < 0.001$.

(E) Left panel: a representative ganglion with 9 sweet-responding neurons. Fluorescence amplitudes were pseudocolored according to ΔF/F. The cartoon (right panel) illustrates the location of the responding neurons, cranial nerve VII (CN VII), and the greater superficial petrosal (GSP) nerve. The bar graph shows the response profile of GCaMP6-expressing Spon1-Cre ganglion neurons: sour, 50 mM citric acid; sweet, 30 mM AceK; salty, 60 mM NaCl; bitter, 5 mM quinine. n = 8 animals, 73 neurons imaged (>50 responded to sweet alone).

(F) Penk-expressing ganglion neurons represent sour taste. Left panel: a representative ganglion with 4 acid-responding neurons. Fluorescence amplitudes were pseudocolored according to ΔF/F. The bar graph shows the response profile of GCaMP6-expressing Penk-Cre ganglion neurons: sour, 50 mM citric acid; sweet: 30 mM AceK; salty, 60 mM NaCl; bitter, 5 mM quinine. n = 6, 38 neurons were imaged, more than 30 responded to sour alone.

define the sour-selective population (Figure 4F). Collectively, these results identified ganglion neurons mediating each of the five basic taste qualities, revealed genetic markers substantiating the cellular and functional segregation of taste at the periphery (Barretto et al., 2015; Lee et al., 2017), and uncovered Penk-expressing neurons as the sour-responding population.

A Dedicated Population of Sour-Sensing Neurons in the Brain

One of the principal brain stations receiving neural signals from the periphery, both from internal (e.g., interoception; Andersson, 1972) and external sensory stimuli (e.g., taste) is the NST in the brain stem (Umans and Liberles, 2018; Yarmolinsky et al., 2009); this nucleus functions as a hub, collecting information from the body and distributing it to subcortical and cortical brain centers. Gustatory information from the periphery accesses the brain by targeting the rostral nucleus of the solitary tract (rNST) (Spector and Travers, 2005; Yarmolinsky et al., 2009).

We infected neurons in the rNST with an adeno-associated virus (AAV) expressing GCaMP6s under a generic synapsin promoter (McLean et al., 2014; Schoch et al., 1996) so as to be expressed in all classes of neurons, and then used fiber photometry (Gunaydin et al., 2014) to record population-level, tastant-evoked responses from GCaMP-expressing cells (Figure 5A). Our results (Figure 5B, top row) showed robust, time-locked, tastant-evoked responses for the different taste stimuli, including sour. These results corroborate the rNST as a neural station for the different taste qualities (Spector and Travers, 2005). However, fiber photometry does not provide cellular-level resolution, so at this stage it is not possible to conclude whether the signals arise from different cell types singularly tuned to each quality or from subpopulations of neurons, each responding to multiple taste stimuli (Roper and Chaudhari, 2017).

To determine whether there is a unique population of neurons in the rNST representing sour taste independent of all other taste qualities or whether the labeled line carrying sour signals from the tongue and taste ganglia breaks down when it goes from

Please cite this article in press as: Zhang et al., Sour Sensing from the Tongue to the Brain, Cell (2019), https://doi.org/10.1016/j.cell.2019.08.031

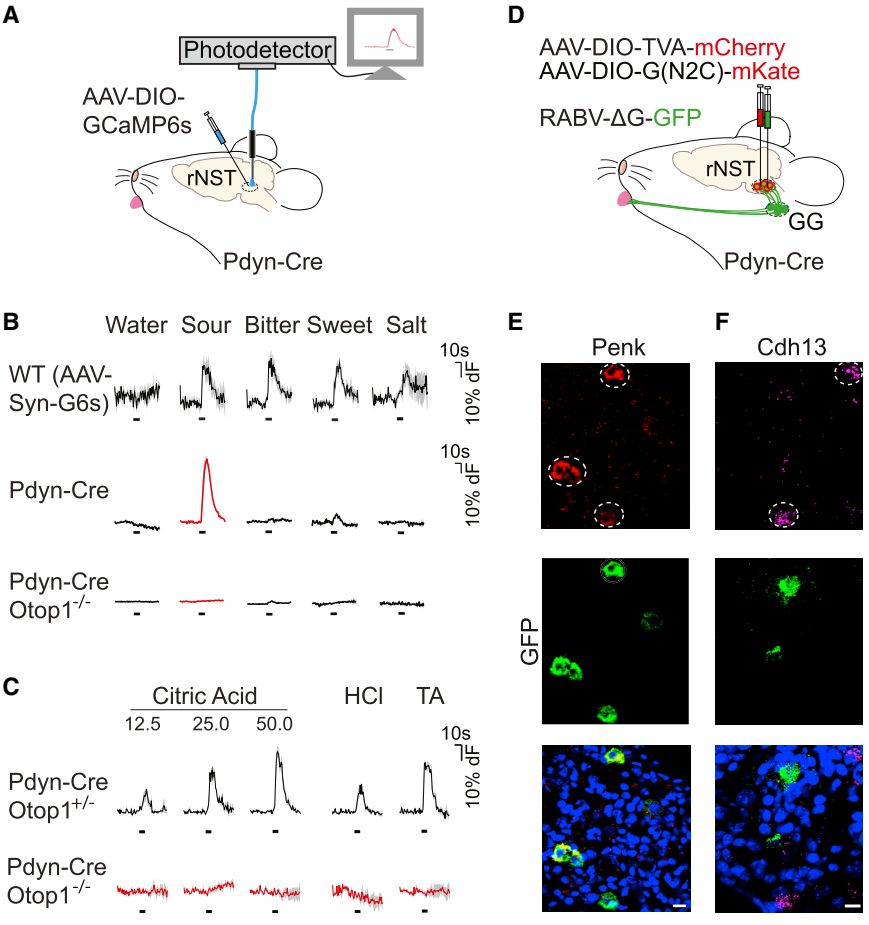

Figure 5. Pdyn Marks a Dedicated Population of Sour-Sensing Neurons in the Brain Stem

(A) Schematic illustrating fiber photometry experiments to monitor tastant-evoked response of Pdyn neurons in the rNST. rNST sour neurons were targeted with GCaMP6s by injection of an AAV-DIO-GCaMP6s in Pdyn-Cre animals. See Figure S5 for staining of neurons and the position of recording fibers).

(B) Top traces: tastant-evoked responses of rNST neurons expressing a synapsin-driven GCaMP6s reporter; note robust responses to all taste stimuli. Center traces: responses of animals expressing the GCaMP6s reporter (AAV-DIO-GCaMP6s) in Pdyn-Cre neurons of the rNST. Note selective responses only to sour stimuli. Bottom traces: responses from Pdyn-expressing GCaMP6s neurons are absent in animals lacking the Otop1sour taste receptor. Traces were aligned to the time of tastant presentation (black bars below). Tastants: 50 mM citric acid, 5 mM quinine, 20 mM AceK, 60 mM NaCl; n = 4 animals per group. Quantifications are shown in Figure S6.

(C) Dose response of Pdyn-expressing sour neurons. Note that all of the responses are abolished in Otop1$^{-/-}$ knockout animals. Quantifications are shown in Figure S6.

(D) Schematic of retrograde monosynaptic tracing. The rostral NSTs of Pdyn-Cre animals were bilaterally infected with AAV-DIO-TVA-mCherry and AAV-DIO-G(N2C)-mKate, followed by infection with RABV-ΔG-GFP.

(E) RNA fluorescence *in situ* hybridization (FISH) for Penk (red, top panel) and GFP (center panel), demonstrating that neurons receiving the transsynaptic viral reporter in the ganglion (labeled in green) are sour Penk-expressing neurons. Bottom panel: the overlap. One section of a geniculate ganglion is shown. n = 6 ganglia; 64 Penk^{+} cells and more than 85% co-labeled with GFP from the retrograde reporter virus; 75 GFP+ cells, and 75% co-labeled with Penk (this number is an underestimate because GFP *in situ* signals are much stronger than endogenous Penk RNA signals). Scale bar, 10 μm.

(F) Control *in situ* using a different ganglion marker (Cdh13 marking bitter neurons, magenta), demonstrating no co-expression with the retrograde transsynaptic reporter (green) originating from Pdyn-expressing neurons in the rNST. Bottom panel: the overlap. One section of a geniculate ganglion is shown. n = 6 ganglia; 30 Cdh13^{+} cells and only 1 co-labeled with GFP from the retrograde reporter virus (3%); 43 GFP^{+} cells but only 1 co-labeled with Cdh13 (2%). Scale bar, 10 μm.

the periphery to the CNS (Ohla et al., 2019), we profiled the rNST for distinct cell types by searching the Allen Brain Atlas for unique genetic markers. Our results demonstrated that prodynorphin-expressing neurons (Pdyn) (Krashes et al., 2014) marked by a Pdyn-Cre construct driving GCaMP6s respond selectively to sour taste stimuli (Figure 5B, center row). Importantly, as would be expected for finely tuned sour taste neurons, the responses are dose-dependent and highly specific to acid stimuli (Figure 5C), with kinetics that match the time course of stimulus onset and decay.

We hypothesized that, if Pdyn-neurons in the rNST represent the taste of sour in the brain stem, then they should receive direct input from the geniculate ganglion neurons coding for sour taste (marked by the Penk gene; Figure 4F). Furthermore, all sour-evoked activity in these Pdyn-positive neurons should be dependent on the function of Otop1 in sour TRCs.

We used a retrograde reporter virus to determine the identity of the ganglion neurons providing synaptic input to the sour-tuned rNST neurons. We infected Pdyn-Cre neurons in the rNST with AAV viruses carrying three different genes used for synaptic tracing (Reardon et al., 2016; Wickersham et al., 2007a, 2007b; Figure 5D): a Cre-dependent viral receptor (TVA, avian tumor virus receptor A) for restricting infection of the transsynaptic reporter virus to Pdyn-positive rNST neurons, a glycoprotein coat gene (G) required for viral packaging and transfer (to restrict transfer monosynaptically), and red fluorescent tags (mKate and mCherry) to mark the starting infected cells in the rNST (referred to as starter cells). Two weeks after this initial infection, the brain stem was infected with the retrograde rabies virus, RABV-ΔG-GFP (Reardon et al., 2016; Wickersham et al., 2007a, 2007b). The infected rNST cells were expected to express the red and green reporters, but their presynaptic partners, following transsynaptic transfer to the ganglion, should only express GFP derived from the transsynaptically transferred RABV-ΔG-GFP virus. Our results (Figures 5E and S5C) demonstrated efficient transfer of the rabies reporter from the rNST to the geniculate ganglion and showed that GFP-labeled neurons in the ganglion were also labeled by the sour-specific marker

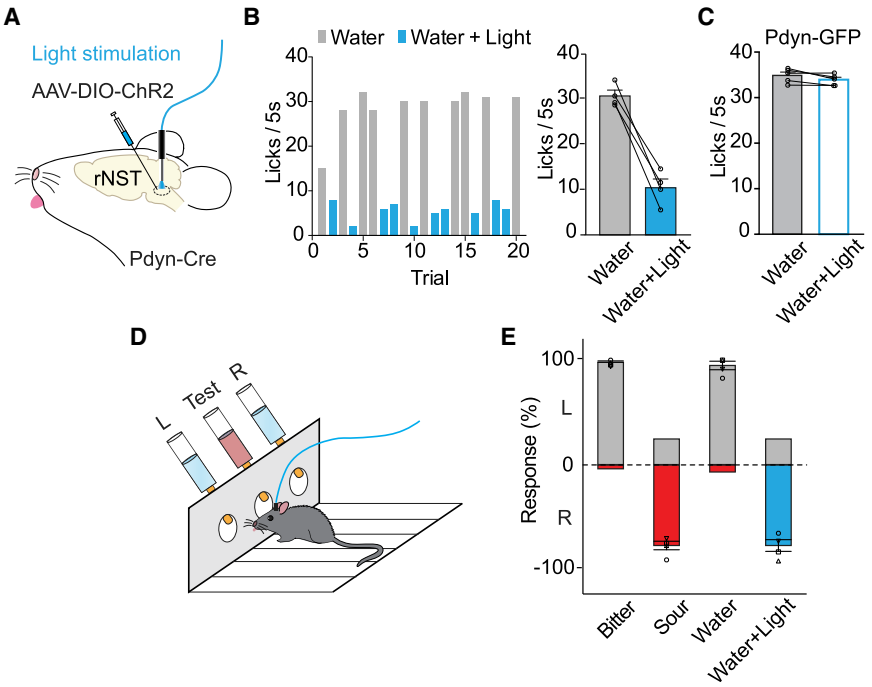

Figure 6. Activation of Pdyn-Labeled Neurons in the Brain Stem

(A) Optogenetic stimulation strategy. Pdyn-expressing neurons in the rNST (Pdyn-Cre animals) were transduced with AAV-DIO-ChR2; stimulating optical fibers were implanted above the rNST.

(B) Representative histograms showing licking events in the presence (blue) or absence (gray) of light stimulation. Left panel: sample session; note the suppression of licking during laser-on trials. Right panel: quantitation of licking responses with and without light stimulation of Pdyn-expressing neurons in the rNST. Values are means ± SEM. n = 4 mice, paired t test, p = 0.0024. Ingestion of water is not required for light-dependent suppression because it is still observed in "dry lick" experiments (Figure S6E).

(C) Control Pdyn-Cre animals injected with AAV-DIO-GFP (Pdyn-GFP). Values are means ± SEM. n = 5 mice.

(D) Schematic of the three-port behavioral test. In each trial, a mouse had to lick a randomly presented tastant from the middle port and then go to either the left or right port to report its identity. During training and testing, the middle port dispensed either 20 mM citric acid (sour), 1 mM quinine (bitter), or water. A session consisted of 10 trials of water, 10 trials of water and light, 33 trials of sour, and 33 trials of bitter, presented in pseudorandom order (STAR Methods). In the example shown, animals were trained to go to the left (L) for bitter and for water trials and to the right (R) for sour trials.

(E) Summary histograms proving that trained animals can identify the different stimuli with high reliability and that optogenetic stimulation of Pdyn neurons in the rNST was recognized as a sour stimulus (~75% accuracy, blue bar). Values are means ± SEM. n = 4 mice, one-way ANOVA (water and light versus water, p = 0.0012; water and light versus sour, p = 0.9979).

Penk by *in situ* hybridization experiments (Figure 5E). These results proved that Pdyn sour-responding neurons in the rNST indeed receive direct and selective input from sour ganglion neurons (see figure legends and STAR Methods for details).

A final prediction was that all sour-evoked activity in Pdyn-positive neurons should be dependent on the function of the OTOP1 ion channel in the sour TRCs. Therefore, we examined responses of Pdyn-positive neurons in the rNST in the background of an Otop1 homozygous knockout mutation (Pdyn-Cre:GCaMP6/Otop1$^{-/-}$). Indeed, GCaMP6-expressing Pdyn neurons in the rNST no longer responded to sour stimuli (Figures 5B, 5C, and S6).

Activation of Pdyn-Expressing Neurons in the Brain Stem Elicit Aversion and Sour Recognition

An important expectation from these studies is that activation of Pdyn neurons in the rNST should evoke prototypical sour-induced behaviors normally evoked by oral stimulation of sour-sensing TRCs. Two key predictions would be that optogenetic activation of rNST sour neurons should trigger aversive responses just as sour chemicals would and that, in a taste discrimination assay, animals should recognize the optogenetic signal as a sour stimulus even when they are drinking only water.

We infected Pdyn-Cre neurons in the rNST with an AAV carrying a Cre-dependent channelrhodopsin-2 (ChR2) construct, implanted optical fibers over the rNST, and assayed the effect of ChR2 activation (Figure 6A). In these experiments, motivated thirsty animals were subjected to multiple water-only trials, but in half of those trials, the Pdyn-neurons were light-activated upon contact of the tongue with the waterspout. Because the laser shutter was placed under contact-licking operation, the animals had control of their own stimulation and therefore were expected to continue to lick when light stimulation elicited attraction but to immediately terminate licking when the light stimulation elicited aversion (Peng et al., 2015). Figure 6B shows that photostimulation of the sour neurons in the rNST evoked reliable stimulus-dependent cessation of licking (whereas activation of Pdyn cells expressing a control GFP had no effect; Figure 6C).

Next, we trained mice to report the identity of a test tastant using a three-port arena (Figure 6D). In this assay, thirsty mice learned to sample a tastant from a center spout (providing random presentations of water, a sour or a bitter solution), and then report its identity either by going to the right or left port; a correct response was rewarded with 4 s of water, whereas an incorrect response received a time-out (in our tests, water and bitter were always associated with the same reward port and sour with the opposite one; see STAR Methods for details). This learned behavior requires that the animal samples the center port, recognizes the identity of the tastant, and executes the appropriate choice in each trial. Following 20–30 sessions of training, animals learned to report the identity of each stimulus (sour, bitter, and water) with more than ~80% accuracy in hundreds of randomized trials (Figure 6E). Importantly, both of the test tastants (sour and bitter) were aversive but required opposite ports, so the animals cannot use valence alone to guide their responses (Peng et al., 2015). Then we examined whether direct optogenetic activation of Pdyn-expressing neurons is also

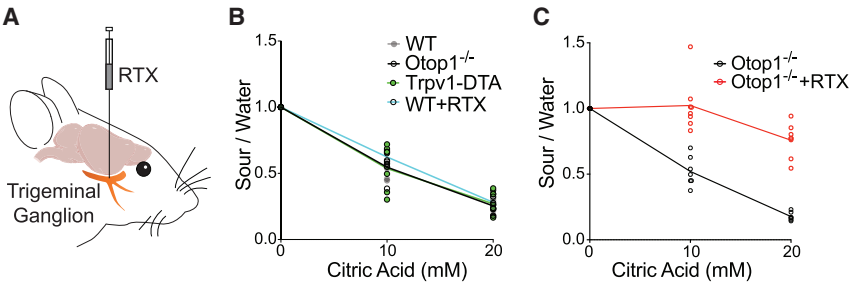

Figure 7. The Sour Taste Pathway Works Together with the Somatosensory System to Trigger Aversive Responses to Acid Stimuli

(A) Cartoon illustrating a trigeminal ganglion with some orofacial projections. The Trpv1-expressing somatosensory neurons in the trigeminal ganglia were ablated by bilateral injection of resiniferatoxin (RTX; STAR Methods).

(B) Behavioral aversion to a sour stimulus in the WT control (n = 4), Otop1$^{-/-}$ (n = 4), Trpv1-DTA (n = 5), and WT animals injected with RTX (WT+RTX, n = 4). Shown are preference ratios calculated as the number of licks to sour stimuli divided by the number of licks to water (sour/water). Two-way ANOVA, no significant differences between any of the groups.

(C) Behavioral aversion to a sour stimulus in Otop1$^{-/-}$ (black, n = 7) versus Otop1$^{-/-}$ animals bilaterally injected with RTX (Otop1$^{-/-}$ + RTX, n = 4 tested in 8 separate sessions). Multiple unpaired t tests, $p < 0.001$ for both concentrations. Otop1$^{-/-}$ mutants shown here are a different cohort of animals than the Otop1$^{-/-}$ mutants shown in (B) (also matched for sex and age). We suggest that the remaining aversion detected at higher concentrations of citric acid in Otop1$^{-/-}$ + RTX animals was due to the 20%–30% of Trpv1-expressing neurons that survived the trigeminal RTX injection (Figure S7); similar numbers of neurons survived in control Trpv1-DTA animals (Figure S7).

recognized as a sour stimulus; if light and the chemical tastant evoke similar percepts, then light stimulation will generalize to the learned responses associated with the orally supplied sour stimulus. Indeed, our results demonstrated that animals reliably reported stimulation of Pdyn-expressing neurons in the rNST as a sour stimulus even though laser activation was only linked to the presentation of water (Figure 6E).

The Sour Taste Pathway Works Together with the Somatosensory System to Trigger Aversive Responses to Acid Stimuli

It has been known for a long time that animals lacking sour TRCs (e.g., expressing diphtheria toxin in Pkd2l1 cells) (Huang et al., 2006) still display strong aversion to acids even though physiological responses from sour TRCs are completely abolished (Huang et al., 2006). How is this aversion mediated? In addition to acid-sensing TRCs, the oral cavity is also richly innervated by trigeminal somatosensory neurons that respond to acid (Yarmolinsky et al., 2016). Thus, we reasoned that the repulsion seen in animals lacking sour taste may be mediated by the somatosensory system (Caterina et al., 1997; Julius, 2013). We generated animals where we chemically ablated Trpv1-expressing neurons in the trigeminal ganglion (Figure 7A) and examined their behavioral responses to acid both in the absence and in the presence of a homozygous Otop1$^{-/-}$ mutant genetic background. To chemically ablate somatosensory acid-responding neurons, we bilaterally injected the trigeminal ganglia with resiniferatoxin (RTX), a strong agonist of Trpv1 known to kill Trpv1-expressing neurons (Mishra and Hoon, 2010; Olah et al., 2001). As a comparison for the degree of ablation, we also engineered animals expressing diphtheria toxin (DTA) in Trpv1 neurons. Our results demonstrated that more than 70% of Trpv1-positive neurons were absent in DTA animals and were ablated after RTX treatment (Figure S7). As anticipated, these animals still exhibited normal aversion to acid stimuli (Figure 7B) because they still harbor the full complement of sour-tasting TRCs. However, when we ablated trigeminal Trpv1-expressing neurons in animals that also lacked the OTOP1 sour taste receptor, they exhibited a major loss of behavioral aversion to acid (Figure 7C); these animals consumed a lower concentration of acid as effectively as water and drank the higher concentration nearly as robustly (see figure legends for details). Together, these results establish the somatosensory and taste systems as co-mediators of acid-evoked aversion and explain why animals deficient in sour taste still exhibit strong aversion to acid stimuli. We suggest that the incomplete ablation of TRPV1 neurons (Figure S7) and the minor sensitivity from T2R cells (Barretto et al., 2015; Oka et al., 2013) may be responsible for the residual behavioral responses in Otop1$^{-/-}$ RTX-treated mice.

DISCUSSION

Otopetrins are a family of proton-conducting channels first identified in the mammalian vestibular system (Hughes et al., 2007, 2008). Mouse strains bearing spontaneously occurring (missense) mutations in Otopetrin-1 exhibit defects in otolith development and consequently display behavioral problems in balance and the sensing of acceleration and gravity (Hurle et al., 2003; Kim et al., 2011; Lane, 1986; Ornitz et al., 1998). Recent studies showed that Otop1 is also expressed in sour TRCs and comprehensively described their proton-conducting and physiological properties in cell-based assays both in WT and in mutant animals (Tu et al., 2018). These pioneering studies by Liman and coworkers (Tu et al., 2018) strongly supported Otop1 as a component of the sour-sensing machinery. Here, we engineered loss-of-function mutations in the Otop1 gene and demonstrated a selective loss of acid responses from sour-sensing TRCs without affecting the other taste modalities. These results proved that OTOP1 is an essential component of sour taste signaling. Then we engineered animals with sweet TRCs expressing OTOP1 (i.e., T1R3-Otop1) and showed that sweet cells responded to sour tastants, formally validating OTOP1 as the sour taste receptor.

The taste system has emerged as one of the best examples of labeled line coding in the mammalian nervous system. Although hard-wired sensory maps have long been described in invertebrates (Harris et al., 2015; Yarmolinsky et al., 2009), the demonstration of their generality in mammals is a recent advance. Indeed, recent studies have shown that it is possible to engineer animals with rewired taste labeled lines, so that sweet TRCs connect to bitter neurons or vice versa (Barretto et al., 2015; Lee et al., 2017). Most relevantly, activation of TRCs in the tongue (Mueller

et al., 2005; Zhao et al., 2003) or direct stimulation of the sweet and bitter taste cortex triggers pre-determined actions and behaviors (like attraction to sweet and aversion to bitter) independent of any learning or experience (Peng et al., 2015). This sharply contrasts the logic of coding in the olfactory system, where most odors carry no innate value but are afforded meaning by learning and experience (Choi et al., 2011). In this paper, we defined the genetic identity of sweet, bitter, umami, salty, and sour neurons in taste ganglia. These results expose the five labeled lines mediating every one of the five basic taste qualities at the periphery.

In the brain stem, we showed that sour taste is represented by its own dedicated population of neurons. We demonstrated that Pdyn-expressing neurons in the rNST are selectively tuned to sour taste and that their optogenetic activation elicits immediate taste aversion just as a sour chemical on the tongue would evoke. Significantly, in a learned taste behavioral assay, activation of Pdyn-expressing neurons is recognized and reported as a sour stimulus. These experiments illustrate how direct control of sour neurons in the brain can evoke specific, reliable, and robust behaviors symbolic of the natural responses to the chemical tastant.

In the future, it will be of great interest to identify the neurons representing each of the basic tastes from the rNST to the parabrachial nucleus (Fu et al., 2019) and from the thalamus to the cortex (Chen et al., 2011) and examine how attractive and aversive tastes are organized and modulated by the internal state and how the different taste qualities come together to orchestrate flavor.

STAR★METHODS

Detailed methods are provided in the online version of this paper and include the following:

- KEY RESOURCES TABLE
- LEAD CONTACT AND MATERIALS AVAILABILITY
- EXPERIMENTAL MODEL AND SUBJECT DETAILS
  - Generation of gene knockout and knockin animals
  - Animals
- METHOD DETAILS
  - Nerve recording
  - Immunostainings
  - Viral infection and optic fiber implantation
  - Calcium imaging and analysis
  - Cell isolation and sequencing library construction
  - Bulk and single cell RNA-seq analysis
  - Gustometer behavior analysis
  - Fiber photometry
  - Retrograde monosynaptic tracing
  - Fluorescent *in situ* hybridization
  - Optogenetic stimulation in lick preference assays
  - Three-port taste-recognition assay
  - Trigeminal microinjection
- QUANTIFICATION AND STATISTICAL ANALYSIS
- DATA AND CODE AVAILABILITY

SUPPLEMENTAL INFORMATION

Supplemental Information can be found online at https://doi.org/10.1016/j.cell.2019.08.031.

ACKNOWLEDGMENTS

We are indebted to Zaiqi Wu for her extraordinary help with mouse engineering. We thank Nick Ryba for experimental suggestions and helpful comments, Robert Barretto and Lindsey Macpherson for help with calcium imaging, Yueqing Peng for help with nerve recording, and Hershy Fishman for help with animals and histology. We particularly acknowledge Rahul Satija and Tom Maniatis for insightful comments and generous help with scRNA-seq and analysis. We thank Yasuo Mori for the kind gift of Trpm2 gene knockout animals and Sabastian Poliak and Amy Norovich for the generous gift of Cdh13::CreER animals. We also thank members of the Zuker lab for helpful discussions; David Yarmolinsky and Nick Ryba for generating the P2rx-Cre lines and general advice; and the talented undergraduates Enoch Jiang, Helen Zhang, and Crystal Richards for their contribution to various aspects of this work. J.Z. was supported by a postdoctoral fellowship from The Jane Coffin Childs Memorial Fund for Medical Research. S.O. was a researcher in Tom Maniatis's laboratory at Columbia University. C.S.Z. is an investigator of the Howard Hughes Medical Institute and a Senior Fellow at the Janelia Farm Research Campus.

AUTHOR CONTRIBUTIONS

J.Z. and H.J. designed the study, carried out the experiments, and analyzed data. W.Z. performed nerve recording, mouse engineering, and behavioral tests. C.D. isolated single neurons for RNA-seq. S.O. analyzed RNA-seq data. M.Y. performed animal behavioral tests. C.S.Z. designed the study and analyzed data. C.S.Z. and J.Z. wrote the paper.

DECLARATION OF INTERESTS

The authors declare no competing interests.

Received: June 17, 2019
Revised: August 4, 2019
Accepted: August 15, 2019
Published: September 19, 2019

REFERENCES

Anders, S., and Huber, W. (2010). Differential expression analysis for sequence count data. Genome Biol. *11*, R106.

Anders, S., Pyl, P.T., and Huber, W. (2015). HTSeq–a Python framework to work with high-throughput sequencing data. Bioinformatics *31*, 166–169.

Andersson, B., Fillenz, M., Hellon, R.F., Howe, A., Leek, B.F., Neil, E., Paintal, A.S., and Widdicombe, J.G. (1972). Enteroceptors. In Handbook of Sensory Physiology, E. Neil, ed. (Springer), p. 233.

Bachmanov, A.A., Li, X., Reed, D.R., Ohmen, J.D., Li, S., Chen, Z., Tordoff, M.G., de Jong, P.J., Wu, C., West, D.B., et al. (2001). Positional cloning of the mouse saccharin preference (Sac) locus. Chem. Senses *26*, 925–933.

Barretto, R.P., Gillis-Smith, S., Chandrashekar, J., Yarmolinsky, D.A., Schnitzer, M.J., Ryba, N.J., and Zuker, C.S. (2015). The neural representation of taste quality at the periphery. Nature *517*, 373–376.

Basu, R., Taylor, M.R., and Williams, M.E. (2015). The classic cadherins in synaptic specificity. Cell Adhes. Migr. *9*, 193–201.

Brockschnieder, D., Pechmann, Y., Sonnenberg-Riethmacher, E., and Riethmacher, D. (2006). An improved mouse line for Cre-induced cell ablation due to diphtheria toxin A, expressed from the Rosa26 locus. Genesis *44*, 322–327.

Butler, A., Hoffman, P., Smibert, P., Papalexi, E., and Satija, R. (2018). Integrating single-cell transcriptomic data across different conditions, technologies, and species. Nat. Biotechnol. *36*, 411–420.

Caterina, M.J., Schumacher, M.A., Tominaga, M., Rosen, T.A., Levine, J.D., and Julius, D. (1997). The capsaicin receptor: a heat-activated ion channel in the pain pathway. Nature *389*, 816–824.

Challis, R.C., and Ma, M. (2016). Sour taste finds closure in a potassium channel. Proc. Natl. Acad. Sci. USA *113*, 246–247.

Chandrashekar, J., Yarmolinsky, D., von Buchholtz, L., Oka, Y., Sly, W., Ryba, N.J., and Zuker, C.S. (2009). The taste of carbonation. Science *326*, 443–445.

Chandrashekar, J., Kuhn, C., Oka, Y., Yarmolinsky, D.A., Hummler, E., Ryba, N.J., and Zuker, C.S. (2010). The cells and peripheral representation of sodium taste in mice. Nature *464*, 297–301.

Chen, X., Gabitto, M., Peng, Y., Ryba, N.J., and Zuker, C.S. (2011). A gustotopic map of taste qualities in the mammalian brain. Science *333*, 1262–1266.

Chen, T.W., Wardill, T.J., Sun, Y., Pulver, S.R., Renninger, S.L., Baohan, A., Schreiter, E.R., Kerr, R.A., Orger, M.B., Jayaraman, V., et al. (2013). Ultrasensitive fluorescent proteins for imaging neuronal activity. Nature *499*, 295–300.

Choi, G.B., Stettler, D.D., Kallman, B.R., Bhaskar, S.T., Fleischmann, A., and Axel, R. (2011). Driving opposing behaviors with ensembles of piriform neurons. Cell *146*, 1004–1015.

Coste, B., Mathur, J., Schmidt, M., Earley, T.J., Ranade, S., Petrus, M.J., Dubin, A.E., and Patapoutian, A. (2010). Piezo1 and Piezo2 are essential components of distinct mechanically activated cation channels. Science *330*, 55–60.

D'Autréaux, F., Coppola, E., Hirsch, M.R., Birchmeier, C., and Brunet, J.F. (2011). Homeoprotein Phox2b commands a somatic-to-visceral switch in cranial sensory pathways. Proc. Natl. Acad. Sci. USA *108*, 20018–20023.

Dahl, M., Erickson, R.P., and Simon, S.A. (1997). Neural responses to bitter compounds in rats. Brain Res. *756*, 22–34.

Danilova, V., and Hellekant, G. (2003). Comparison of the responses of the chorda tympani and glossopharyngeal nerves to taste stimuli in C57BL/6J mice. BMC Neurosci. *4*, 5.

Dickinson, M.E., Flenniken, A.M., Ji, X., Teboul, L., Wong, M.D., White, J.K., Meehan, T.F., Weninger, W.J., Westerberg, H., Adissu, H., et al.; International Mouse Phenotyping Consortium; Jackson Laboratory; Infrastructure Nationale PHENOMIN, Institut Clinique de la Souris (ICS); Charles River Laboratories; MRC Harwell; Toronto Centre for Phenogenomics; Wellcome Trust Sanger Institute; RIKEN BioResource Center (2016). High-throughput discovery of novel developmental phenotypes. Nature *537*, 508–514.

Dobin, A., Davis, C.A., Schlesinger, F., Drenkow, J., Zaleski, C., Jha, S., Batut, P., Chaisson, M., and Gingeras, T.R. (2013). STAR: ultrafast universal RNA-seq aligner. Bioinformatics *29*, 15–21.

Dvoryanchikov, G., Hernandez, D., Roebber, J.K., Hill, D.L., Roper, S.D., and Chaudhari, N. (2017). Transcriptomes and neurotransmitter profiles of classes of gustatory and somatosensory neurons in the geniculate ganglion. Nat. Commun. *8*, 760.

Fu, O., Iwai, Y., Kondoh, K., Misaka, T., Minokoshi, Y., and Nakajima, K.I. (2019). SatB2-Expressing Neurons in the Parabrachial Nucleus Encode Sweet Taste. Cell Rep. *27*, 1650–1656.e4.

Glendinning, J.I., Gresack, J., and Spector, A.C. (2002). A high-throughput screening procedure for identifying mice with aberrant taste and oromotor function. Chem. Senses *27*, 461–474.

Gunaydin, L.A., Grosenick, L., Finkelstein, J.C., Kauvar, I.V., Fenno, L.E., Adhikari, A., Lammel, S., Mirzabekov, J.J., Airan, R.D., Zalocusky, K.A., et al. (2014). Natural neural projection dynamics underlying social behavior. Cell *157*, 1535–1551.

Harris, D.T., Kallman, B.R., Mullaney, B.C., and Scott, K. (2015). Representations of Taste Modality in the Drosophila Brain. Neuron *86*, 1449–1460.

Hashimshony, T., Wagner, F., Sher, N., and Yanai, I. (2012). CEL-Seq: single-cell RNA-Seq by multiplexed linear amplification. Cell Rep. *2*, 666–673.

Hashimshony, T., Senderovich, N., Avital, G., Klochendler, A., de Leeuw, Y., Anavy, L., Gennert, D., Li, S., Livak, K.J., Rozenblatt-Rosen, O., et al. (2016). CEL-Seq2: sensitive highly-multiplexed single-cell RNA-Seq. Genome Biol. *17*, 77.

Horio, N., Yoshida, R., Yasumatsu, K., Yanagawa, Y., Ishimaru, Y., Matsunami, H., and Ninomiya, Y. (2011). Sour taste responses in mice lacking PKD channels. PLoS ONE *6*, e20007.

Huang, A.L., Chen, X., Hoon, M.A., Chandrashekar, J., Guo, W., Tränkner, D., Ryba, N.J., and Zuker, C.S. (2006). The cells and logic for mammalian sour taste detection. Nature *442*, 934–938.

Huang, Y.A., Stone, L.M., Pereira, E., Yang, R., Kinnamon, J.C., Dvoryanchikov, G., Chaudhari, N., Finger, T.E., Kinnamon, S.C., and Roper, S.D. (2011). Knocking out P2X receptors reduces transmitter secretion in taste buds. J. Neurosci. *31*, 13654–13661.

Hughes, I., Blasiole, B., Huss, D., Warchol, M.E., Rath, N.P., Hurle, B., Ignatova, E., Dickman, J.D., Thalmann, R., Levenson, R., and Ornitz, D.M. (2004). Otopetrin 1 is required for otolith formation in the zebrafish Danio rerio. Dev. Biol. *276*, 391–402.

Hughes, I., Saito, M., Schlesinger, P.H., and Ornitz, D.M. (2007). Otopetrin 1 activation by purinergic nucleotides regulates intracellular calcium. Proc. Natl. Acad. Sci. USA *104*, 12023–12028.

Hughes, I., Binkley, J., Hurle, B., Green, E.D., Sidow, A., and Ornitz, D.M.; NISC Comparative Sequencing Program (2008). Identification of the Otopetrin Domain, a conserved domain in vertebrate otopetrins and invertebrate otopetrin-like family members. BMC Evol. Biol. *8*, 41.

Hurle, B., Ignatova, E., Massironi, S.M., Mashimo, T., Rios, X., Thalmann, I., Thalmann, R., and Ornitz, D.M. (2003). Non-syndromic vestibular disorder with otoconial agenesis in tilted/mergulhador mice caused by mutations in otopetrin 1. Hum. Mol. Genet. *12*, 777–789.

Julius, D. (2013). TRP channels and pain. Annu. Rev. Cell Dev. Biol. *29*, 355–384.

Karai, L., Brown, D.C., Mannes, A.J., Connelly, S.T., Brown, J., Gandal, M., Wellisch, O.M., Neubert, J.K., Olah, Z., and Iadarola, M.J. (2004). Deletion of vanilloid receptor 1-expressing primary afferent neurons for pain control. J. Clin. Invest. *113*, 1344–1352.

Kim, E., Hyrc, K.L., Speck, J., Salles, F.T., Lundberg, Y.W., Goldberg, M.P., Kachar, B., Warchol, M.E., and Ornitz, D.M. (2011). Missense mutations in Otopetrin 1 affect subcellular localization and inhibition of purinergic signaling in vestibular supporting cells. Mol. Cell. Neurosci. *46*, 655–661.

Krashes, M.J., Shah, B.P., Madara, J.C., Olson, D.P., Strochlic, D.E., Garfield, A.S., Vong, L., Pei, H., Watabe-Uchida, M., Uchida, N., et al. (2014). An excitatory paraventricular nucleus to AgRP neuron circuit that drives hunger. Nature *507*, 238–242.

Lane, P. (1986). Tilted (tlt). Mouse News Lett. *75*, 28.

Lee, H., Macpherson, L.J., Parada, C.A., Zuker, C.S., and Ryba, N.J.P. (2017). Rewiring the taste system. Nature *548*, 330–333.

Leffler, A., Mönter, B., and Koltzenburg, M. (2006). The role of the capsaicin receptor TRPV1 and acid-sensing ion channels (ASICS) in proton sensitivity of subpopulations of primary nociceptive neurons in rats and mice. Neuroscience *139*, 699–709.

Lin, W., Ogura, T., and Kinnamon, S.C. (2002). Acid-activated cation currents in rat vallate taste receptor cells. J. Neurophysiol. *88*, 133–141.

Lin, W., Burks, C.A., Hansen, D.R., Kinnamon, S.C., and Gilbertson, T.A. (2004). Taste receptor cells express pH-sensitive leak K+ channels. J. Neurophysiol. *92*, 2909–2919.

Madisen, L., Zwingman, T.A., Sunkin, S.M., Oh, S.W., Zariwala, H.A., Gu, H., Ng, L.L., Palmiter, R.D., Hawrylycz, M.J., Jones, A.R., et al. (2010). A robust and high-throughput Cre reporting and characterization system for the whole mouse brain. Nat. Neurosci. *13*, 133–140.

Madisen, L., Garner, A.R., Shimaoka, D., Chuong, A.S., Klapoetke, N.C., Li, L., van der Bourg, A., Niino, Y., Egolf, L., Monetti, C., et al. (2015). Transgenic mice for intersectional targeting of neural sensors and effectors with high specificity and performance. Neuron *85*, 942–958.

McLean, J.R., Smith, G.A., Rocha, E.M., Hayes, M.A., Beagan, J.A., Hallett, P.J., and Isacson, O. (2014). Widespread neuron-specific transgene expression in brain and spinal cord following synapsin promoter-driven AAV9 neonatal intracerebroventricular injection. Neurosci. Lett. *576*, 73–78.

Mishra, S.K., and Hoon, M.A. (2010). Ablation of TrpV1 neurons reveals their selective role in thermal pain sensation. Mol. Cell. Neurosci. *43*, 157–163.

Mishra, S.K., Tisel, S.M., Orestes, P., Bhangoo, S.K., and Hoon, M.A. (2011). TRPV1-lineage neurons are required for thermal sensation. EMBO J. *30*, 582–593.

Mueller, K.L., Hoon, M.A., Erlenbach, I., Chandrashekar, J., Zuker, C.S., and Ryba, N.J. (2005). The receptors and coding logic for bitter taste. Nature *434*, 225–229.

Nelson, G., Hoon, M.A., Chandrashekar, J., Zhang, Y., Ryba, N.J., and Zuker, C.S. (2001). Mammalian sweet taste receptors. Cell *106*, 381–390.

Nelson, G., Chandrashekar, J., Hoon, M.A., Feng, L., Zhao, G., Ryba, N.J., and Zuker, C.S. (2002). An amino-acid taste receptor. Nature *416*, 199–202.

Nelson, T.M., Lopezjimenez, N.D., Tessarollo, L., Inoue, M., Bachmanov, A.A., and Sullivan, S.L. (2010). Taste function in mice with a targeted mutation of the pkd1l3 gene. Chem. Senses *35*, 565–577.

Ohla, K., Yoshida, R., Roper, S.D., Di Lorenzo, P.M., Victor, J.D., Boughter, J.D., Fletcher, M., Katz, D.B., and Chaudhari, N. (2019). Recognizing Taste: Coding Patterns Along the Neural Axis in Mammals. Chem. Senses *44*, 237–247.

Oka, Y., Butnaru, M., von Buchholtz, L., Ryba, N.J., and Zuker, C.S. (2013). High salt recruits aversive taste pathways. Nature *494*, 472–475.

Olah, Z., Szabo, T., Karai, L., Hough, C., Fields, R.D., Caudle, R.M., Blumberg, P.M., and Iadarola, M.J. (2001). Ligand-induced dynamic membrane changes and cell deletion conferred by vanilloid receptor 1. J. Biol. Chem. *276*, 11021–11030.

Ornitz, D.M., Bohne, B.A., Thalmann, I., Harding, G.W., and Thalmann, R. (1998). Otoconial agenesis in tilted mutant mice. Hear. Res. *122*, 60–70.

Paxinos, G., and Franklin, K. (2003). The Mouse Brain in Stereotaxic Coordinates, Second Edition (Academic Press).

Peng, Y., Gillis-Smith, S., Jin, H., Tränkner, D., Ryba, N.J., and Zuker, C.S. (2015). Sweet and bitter taste in the brain of awake behaving animals. Nature *527*, 512–515.

Phillips, M.I., and Norgen, R.E. (1970). A rapid method for permanent implantation of intraoral fistula in rats. Behavior Research Methods and Instrumentation *2*, 124.

Poliak, S., Norovich, A.L., Yamagata, M., Sanes, J.R., and Jessell, T.M. (2016). Muscle-type Identity of Proprioceptors Specified by Spatially Restricted Signals from Limb Mesenchyme. Cell *164*, 512–525.

Ranade, S.S., Woo, S.H., Dubin, A.E., Moshourab, R.A., Wetzel, C., Petrus, M., Mathur, J., Bégay, V., Coste, B., Mainquist, J., et al. (2014). Piezo2 is the major transducer of mechanical forces for touch sensation in mice. Nature *516*, 121–125.

Reardon, T.R., Murray, A.J., Turi, G.F., Wirblich, C., Croce, K.R., Schnell, M.J., Jessell, T.M., and Losonczy, A. (2016). Rabies Virus CVS-N2c(ΔG) Strain Enhances Retrograde Synaptic Transfer and Neuronal Viability. Neuron *89*, 711–724.

Richter, T.A., Dvoryanchikov, G.A., Chaudhari, N., and Roper, S.D. (2004). Acid-sensitive two-pore domain potassium (K2P) channels in mouse taste buds. J. Neurophysiol. *92*, 1928–1936.

Roper, S.D., and Chaudhari, N. (2017). Taste buds: cells, signals and synapses. Nat. Rev. Neurosci. *18*, 485–497.

Rousseeuw, P.J., and Croux, C. (1993). Alternatives to the median absolute deviation. J. Am. Stat. Assoc. *88*, 1273–1283.

Sanes, J.R., and Yamagata, M. (2009). Many paths to synaptic specificity. Annu. Rev. Cell Dev. Biol. *25*, 161–195.

Satija, R., Farrell, J.A., Gennert, D., Schier, A.F., and Regev, A. (2015). Spatial reconstruction of single-cell gene expression data. Nat. Biotechnol. *33*, 495–502.

Schoch, S., Cibelli, G., and Thiel, G. (1996). Neuron-specific gene expression of synapsin I. Major role of a negative regulatory mechanism. J. Biol. Chem. *271*, 3317–3323.

Sollars, S.I., and Hill, D.L. (2005). In vivo recordings from rat geniculate ganglia: taste response properties of individual greater superficial petrosal and chorda tympani neurones. J. Physiol. *564*, 877–893.

Spector, A.C., and Travers, S.P. (2005). The representation of taste quality in the mammalian nervous system. Behav. Cogn. Neurosci. Rev. *4*, 143–191.

Stevens, D.R., Seifert, R., Bufe, B., Müller, F., Kremmer, E., Gauss, R., Meyerhof, W., Kaupp, U.B., and Lindemann, B. (2001). Hyperpolarization-activated channels HCN1 and HCN4 mediate responses to sour stimuli. Nature *413*, 631–635.

Tu, Y.H., Cooper, A.J., Teng, B., Chang, R.B., Artiga, D.J., Turner, H.N., Mulhall, E.M., Ye, W., Smith, A.D., and Liman, E.R. (2018). An evolutionarily conserved gene family encodes proton-selective ion channels. Science *359*, 1047–1050.

Ugawa, S., Minami, Y., Guo, W., Saishin, Y., Takatsuji, K., Yamamoto, T., Tohyama, M., and Shimada, S. (1998). Receptor that leaves a sour taste in the mouth. Nature *395*, 555–556.

Ugawa, S., Yamamoto, T., Ueda, T., Ishida, Y., Inagaki, A., Nishigaki, M., and Shimada, S. (2003). Amiloride-insensitive currents of the acid-sensing ion channel-2a (ASIC2a)/ASIC2b heteromeric sour-taste receptor channel. J. Neurosci. *23*, 3616–3622.

Umans, B.D., and Liberles, S.D. (2018). Neural Sensing of Organ Volume. Trends Neurosci. *41*, 911–924.

Voiculescu, O., Charnay, P., and Schneider-Maunoury, S. (2000). Expression pattern of a Krox-20/Cre knock-in allele in the developing hindbrain, bones, and peripheral nervous system. Genesis *26*, 123–126.

Wang, L., Gillis-Smith, S., Peng, Y., Zhang, J., Chen, X., Salzman, C.D., Ryba, N.J.P., and Zuker, C.S. (2018). The coding of valence and identity in the mammalian taste system. Nature *558*, 127–131.

Wickersham, I.R., Finke, S., Conzelmann, K.K., and Callaway, E.M. (2007a). Retrograde neuronal tracing with a deletion-mutant rabies virus. Nat. Methods *4*, 47–49.

Wickersham, I.R., Lyon, D.C., Barnard, R.J., Mori, T., Finke, S., Conzelmann, K.K., Young, J.A., and Callaway, E.M. (2007b). Monosynaptic restriction of transsynaptic tracing from single, genetically targeted neurons. Neuron *53*, 639–647.

Xiao, R., and Xu, X.Z. (2010). Mechanosensitive channels: in touch with Piezo. Curr. Biol. *20*, R936–R938.

Yamamoto, S., Shimizu, S., Kiyonaka, S., Takahashi, N., Wajima, T., Hara, Y., Negoro, T., Hiroi, T., Kiuchi, Y., Okada, T., et al. (2008). TRPM2-mediated Ca2+influx induces chemokine production in monocytes that aggravates inflammatory neutrophil infiltration. Nat. Med. *14*, 738–747.

Yang, H., Wang, H., and Jaenisch, R. (2014). Generating genetically modified mice using CRISPR/Cas-mediated genome engineering. Nat. Protoc. *9*, 1956–1968.

Yarmolinsky, D.A., Zuker, C.S., and Ryba, N.J. (2009). Common sense about taste: from mammals to insects. Cell *139*, 234–244.

Yarmolinsky, D.A., Peng, Y., Pogorzala, L.A., Rutlin, M., Hoon, M.A., and Zuker, C.S. (2016). Coding and Plasticity in the Mammalian Thermosensory System. Neuron *92*, 1079–1092.

Ye, W., Chang, R.B., Bushman, J.D., Tu, Y.H., Mulhall, E.M., Wilson, C.E., Cooper, A.J., Chick, W.S., Hill-Eubanks, D.C., Nelson, M.T., et al. (2016). The K+ channel KIR2.1 functions in tandem with proton influx to mediate sour taste transduction. Proc. Natl. Acad. Sci. USA *113*, E229–E238.

Yogev, S., and Shen, K. (2014). Cellular and molecular mechanisms of synaptic specificity. Annu. Rev. Cell Dev. Biol. *30*, 417–437.

Zhang, Y., Hoon, M.A., Chandrashekar, J., Mueller, K.L., Cook, B., Wu, D., Zuker, C.S., and Ryba, N.J. (2003). Coding of sweet, bitter, and umami tastes: different receptor cells sharing similar signaling pathways. Cell *112*, 293–301.

Zhang, Y., Narayan, S., Geiman, E., Lanuza, G.M., Velasquez, T., Shanks, B., Akay, T., Dyck, J., Pearson, K., Gosgnach, S., et al. (2008). V3 spinal neurons establish a robust and balanced locomotor rhythm during walking. Neuron *60*, 84–96.

Zhao, G.Q., Zhang, Y., Hoon, M.A., Chandrashekar, J., Erlenbach, I., Ryba, N.J., and Zuker, C.S. (2003). The receptors for mammalian sweet and umami taste. Cell *115*, 255–266.

Please cite this article in press as: Zhang et al., Sour Sensing from the Tongue to the Brain, Cell (2019), https://doi.org/10.1016/j.cell.2019.08.031

STAR★METHODS

KEY RESOURCES TABLE

REAGENT or RESOURCE	SOURCE	IDENTIFIER
Antibodies		
Anti-OTOP1	Novus Biologicals	NBP1-86306
Anti-CAR4	R&D Systems	AF2414
Anti-T1R3	Santa Cruz Biotechnology	sc-22458
Bacterial and Virus Strains		
AAV1-Syn-GCaMP6s-WPRE-SV40	Addgene	100843-AAV1
AAV1-Syn-Flex-GCaMP6s-WPRE-SV40	Addgene	100845-AAV1
AAV1-EF1a-ChR2(H132R)-eYFP	Addgene	35507-AAV1
AAV1-DIO-GFP	Addgene	51502-AAV1
AAV1-EF1a-FLEX-TVAmCherry	UNC Vector Core	N/A
AAV1- G(N2C)-mKate	Janelia Viral Core	N/A
RABV-N2C(Delta G)-GFP-EnvA	Janelia Viral Core	N/A
Chemicals, Peptides, and Recombinant Proteins		
Acesulfame K	Sigma-Aldrich	04054
Actidione (Cycloheximide)	Fluka	01810
Citric Acid	Sigma-Aldrich	251275
Hydrochloric acid	Sigma-Aldrich	H1758
Inosine 5′-monophosphate disodium salt hydrate	Sigma-Aldrich	I4625
L-Glutamic acid monopotassium monohydrate	Sigma-Aldrich	49601
Sodium Chloride	Sigma-Aldrich	S5886
Quinine monohydrochloride dihydrate	Sigma-Aldrich	145920
Resiniferatoxin	Santa Cruz Biotechnology	SC-24015
Tartaric acid	Sigma-Aldrich	W304401
Critical Commercial Assays		
Agencourt AMPure XP	Bechman Coulter	A63880
MessageAmp II aRNA Amplification Kit	Invitrogen	AM1751
RNaseOUT Recombinant Ribonuclease Inhibitor	Invitrogen	10777019
RNeasy MinElute Cleanup Kit	QIAGEN	74204
Nextera XT DNA Library Preparation Kit	Illumina	FC-131-1096
SMART-Seq Ultra Low Input RNA Kit	TaKaRa	634891
SuperScript II Reverse Transcriptase	Invitrogen	18064014
T4 Polynucleotide Kinase	NEB	M0201
T4 RNA Ligase 2, truncated	NEB	M0242
TruSeq Small RNA Library Prep Kit	Illumina	RS-200
Deposited Data		
Raw and analyzed data	This paper	GEO: GSE135801
Experimental Models: Organisms/Strains (Mouse)		
Ai9	The Jackson Laboratory	007909
Ai96	The Jackson Laboratory	028866
Cdh4 knockout (B6N(Cg)-Cdh4$^{tm1b(EUCOMM)Wtsi}$/J)	The Jackson Laboratory	025179
Cdh13 knockout (Cdh13::CreER)	Poliak et al., 2016	
Egr2-Cre	The Jackson Laboratory	025744
Penk-IRES2-Cre	The Jackson Laboratory	025112

(*Continued on next page*)

Continued

REAGENT or RESOURCE	SOURCE	IDENTIFIER
Pdyn-IRES-Cre	The Jackson Laboratory	027958
$R26^{floxstop\text{-}TeNT}$	Zhang et al., 2008	N/A
Rosa-DTA	Brockschnieder et al., 2006	N/A
Trpm2 knockout	Yamamoto et al., 2008	N/A
Hcn3 knockout	This paper	N/A
Kcnk1 knockout	This paper	N/A
Kcnk16 knockout	This paper	N/A
Slc38a5 knockout	This paper	N/A
Slc38a11 knockout	This paper	N/A
Otop1 knockout	This paper	N/A
Spon1-IRES-Cre	This paper	N/A
T1R3-Otop1	This paper	N/A
Oligonucleotides		
Guide sequence for Hcn3 knockout: AGGCCCGCGCGGCCTCAGGT	This paper	N/A
Guide sequence for Kcnk1 knockout: CTACCTGGTGTTCGGCGCCG	This paper	N/A
Guide sequence for Kcnk16 knockout: CCAAGTATTGCCCCTGCTTC	This paper	N/A
Guide sequences for Slc38a5 knockout: CCCGTAACCCTGCTACTGGG & AGCTACAGGCAGGAACGCGA	This paper	N/A
Guide sequences for Slc38a11 knockout: ATCTCCGGACATGAACACGG & TCCGGACATGAACACGGA	This paper	N/A
Guide sequences for Otop1 knockout: 1. GACTGAACGTGTTCGTGGCG & CCGCCCCAAGGACACGCACG 2. GTATGGACTGAACGTGTTCG & GCGGTGCACGCGACGGGTGT	This paper	N/A
Guide sequences for Spon1-Cre knockin: AATGGGGGTTCAACTCCCCA & CAATAGTCTTATGATGCCAA	This paper	N/A
Guide sequences for T1R3-Otop1 knockin: GTGTCTGTCACAGCAATTCA & AGACCCATGATAGCCAAAGC	This paper	N/A
Cdh13 *in situ* probe	Advanced Cell Diagnostics	443251
eGFP *in situ* probe	Advanced Cell Diagnostics	400288-C2
Penk *in situ* probe	Advanced Cell Diagnostics	318761
Trpv1 *in situ* probe	Advanced Cell Diagnostics	313331
Recombinant DNA		
Donor vector for Spon1-Cre knockin:pUC57-IRES-Cre (containing Spon1 locus homologous arms)	This paper	N/A
Donor vector for T1R3-Otop1 knockin:pUC57-Otop1 (containing Tas1r3 locus homologous arms)	This paper	N/A
Software and Algorithms		
Arduino	Arduino	https://www.arduino.cc
ImageJ (Fiji)	NIH	https://imagej.net/Fiji
MATLAB	MathWorks	https://www.mathworks.com
Mouse Brain Atlas	Allen Brain Institute	https://alleninstitute.org/
RStudio	R Consortium	https://www.r-project.org
Seurat	The Satija Lab	https://satijalab.org/seurat/

LEAD CONTACT AND MATERIALS AVAILABILITY

Further information and requests for reagents may be directed and will be fulfilled by the Lead Contact, Charles Zuker (cz2195@columbia.edu).

Materials generated in this study, including engineered mice, are available for distribution by contacting Charles Zuker (cz2195@columbia.edu).

EXPERIMENTAL MODEL AND SUBJECT DETAILS

Generation of gene knockout and knockin animals

All gene knockout and knockin mice were generated using CRISPR-Cas9-mediated genome engineering techniques. All mutations were validated by Sanger DNA sequencing. Gene knockout animals including Otop1$^{-/-}$ (Figure 1), Slc38a5$^{-/-}$, Slc38a11$^{-/-}$, Hcn3$^{-/-}$, Kcnk1$^{-/-}$, Kcnk16$^{-/-}$ (Figure S1) were generated by injecting a mixture of Cas9 mRNA (50ng/μl) and gene-specific guide-RNA (sgRNA, 1 or 2 injected, each at 20ng/μl) into the zygotes, as described previously (Yang et al., 2014). For Otop1 knockout animals, two founders were generated and no differences were observed in our experiments (founder 1 is described in detail in Figure S2, founder 2 carries 49 bp deletion in exon 1). As expected, the Otop1$^{-/-}$ homozygous mutant animals exhibited the tilted and balance deficit phenotypes (Hurle et al., 2003; Kim et al., 2011; Lane, 1986; Ornitz et al., 1998). The Slc38a5$^{-/-}$, Slc38a11$^{-/-}$, Hcn3$^{-/-}$, Kcnk1$^{-/-}$, and Kcnk16$^{-/-}$ mutants were only tested for potential deficits in sour taste; no other phenotypes were examined. The sgRNA sequences used to generate the lines are listed in the Key Resources Table, and the schematics used for generating the CRISPR-based mutations are shown in Figures 1, S1, and S2. The loss of OTOP1 protein in the homozygous mutants was verified by immunostaining using OTOP1 antibodies (Figure S2B).

To engineer T1R3-Otop1 knockin animals (Figure 2), a donor vector containing the Tas1r3 homology arms (left and right arms, 2kb each), the coding sequence of murine Otop1, and a BGH polyA 3′ end was synthesized *in vitro*. The Otop1 coding sequences was targeted to be in frame after the ATG start of the Tas1r3 ORF. For injection in zygotes, we used Cas9 mRNA (50ng/μl), gene-specific guide-RNAs (20ng/μl each), and donor vector (5ng/μl) as described previously (Yang et al., 2014). All animals used for the T1R3-Otop1 experiments were validated by Sanger sequencing, demonstrating the insertion of Otop1 at nucleotide +3 (counting from the native T1R3 initiator ATG, Figure S2).

To engineer Spon1-Cre knockin animals (Figure 4E), a vector containing gene-specific homology arms and an IRES-Cre-bGHpoly(A) fragment was synthesized *in vitro* (GenScript). The individual guide sequences are listed in the Key Resources Table. The IRES-Cre driver was targeted immediately downstream of the native Spon1 stop codon. Cas9 mRNA (50ng/μl) and two gene-specific guide-RNAs (20ng/μl each) were co-injected in combination with the targeting vector (5ng/μl).

All sgRNAs were designed using the CRISPR web tool: https://zlab.bio/guide-design-resources; sequences are provided in the Key Resources Table.

Animals

All procedures were carried out in accordance with the US National Institutes of Health (NIH) guidelines for the care and use of laboratory animals, and were approved by the Columbia University Institutional Animal Care and Use Committee. Experiments were carried out using adult mice of age between 2 to 8 months (both male and female). In behavioral assays, animals of similar age and sex composition were used in the control group and the experimental group. All engineered and obtained animals are listed in the Key Resources Table. The Pkd2l1-tdTomato animals, used to isolate sour taste cells for sequencing experiments, were generated by crossing Pkd2l1-Cre (Huang et al., 2006) with the Cre-dependent tdTomato reporter line Ai9 (Madisen et al., 2010). The P2rx3-tdTomato animals, used to isolate single geniculate ganglion neurons for sequencing, were generated by breeding P2rx3-Cre with Ai9 (Madisen et al., 2010). Egr2-TeNT animals (Figure 4B) were generated by breeding Egr2-Cre (The Jackson Laboratory) with R26$^{floxstop\text{-}TeNT}$ (Zhang et al., 2008) animals. To target GCaMP6s expression in specific clusters of geniculate ganglion neurons (Figures 4E and 4F), Spon1-Cre and Penk-Cre (The Jackson Laboratory) mice were bred with Ai96 (Madisen et al., 2015), a Cre-dependent GCaMP6s reporter line obtained from The Jackson Laboratory. Trpv1-DTA animals (Figure 7) were generated by breeding Trpv1-Cre (Mishra et al., 2011) with Rosa-DTA (Brockschnieder et al., 2006).

METHOD DETAILS

Nerve recording

Nerve recording procedures were performed as previously described (Dahl et al., 1997; Nelson et al., 2002). Taste stimuli were presented at a constant flow rate of 6 mL/min for 10 s intervals interspersed by 50 s rinses with artificial saliva (Danilova and Hellekant, 2003). Neural activity was amplified (10,000x) with a Grass P511 AC amplifier (Astro-Med), dititized with Digidata 1440A (Axon Instruments), and integrated with a time constant of 1 s. Each experimental series consisted of the application of 6 tastants bracketed by 2 presentations of 30mM AceK to ensure the stability of the recording. The mean responses to 30mM AceK (Figures 1 and S1C) or 100mM NaCl (Figure S1B) were used to normalize responses, shown in graphs as NR. Control recordings were carried out in C57BL/6J mice.

Tastants used for nerve recordings were: AceK, 30mM; NaCl, 100mM; quinine hydrochloride, 5 mM; monopotassium glutamate + inosine monophosphate, 30 mM + 1 mM, citric acid, 12.5, 25 and 50mM; hydrochloric acid,10mM; tartaric acid, 50mM. AITC was used (Figures 1and S1) to suppress responses from bitter cells as indicated in the figure legends. As described previously (Oka et al., 2013), 3mM AITC was applied to the tongue at 6ml/ml for 5min; the tongue was washed with artificial saliva for 1 min and nerve responses to the same series of taste stimuli were measured; responses before and after AITC were compared for each animal (see Figure S1C). Responses after AITC were recorded within 20min of AITC treatment.

Immunostainings

Animals were euthanized and fixed by intracardiac perfusion with 4% paraformaldehyde solution. Tongues were excised and placed in 30% sucrose solution overnight at 4°C for cryoprotection. Tissue was processed as previously described (Lee et al., 2017), sections were washed in PBS with 0.1% Triton X-100, blocked with 10% donkey serum, incubated with primary antibodies overnight at 4°C, and labeled with fluorescently tagged secondary antibodies for 2h at room temperature. Primary antibodies used were: anti-OTOP1 (Novus Biologicals NBP1-86306, 1:100), anti-CAR4 (R&D Systems AF2414, 1:1000), anti-T1R3 (Santa Cruz Biotechnology sc-22458, 1:200).

Viral infection and optic fiber implantation

Animals were anaesthetized and placed into a stereotaxic frame with a close-loop heating system to maintain body temperature. For calcium imaging experiments described in Figure 1, WT and Otop1$^{-/-}$ animals were bilaterally injected in the rostral NST with an AAV carrying a GCaMP6s expression cassette (AAV1-Syn-GCaMP6s); to maximize the number of labeled neurons in the geniculate ganglion, 6 locations were injected at 30nl each (bregma 6.5mm and 6.3mm; lateral 1.25mm; ventral 4.2mm, 4.0mm and 3.8mm). For optogenetic stimulation experiments, 50 nL of AAV-DIO-ChR2 or AAV-DIO-GFP was injected at coordinate bregma 6.4mm; lateral 1.1mm; ventral 4.0mm. For fiber photometry experiments, 300 nL of AAV1-Syn-GCAMP6s or AAV1-DIO-GCaMP6s were injected at coordinates bregma 6.5 and 6.3mm; lateral 1.0 and 1.2mm; ventral 4.2mm, 4.0mm and 3.8mm). Mice were housed in their home cages for at least two weeks to recover from surgery prior to any experiments.

For optogenetic fiber implants, fibers were custom made (O.D. 200 μm, NA 0.39, Thorlabs) and placed 200-300 μm above the viral injection site. For photometry implants, custom-made fibers were purchased from Doric Lenses (O.D. 400 μm, NA = 0.48) and implanted 0-50 μm above the injection site. All implants were secured onto the skull with dental cement (Lang Dental Manufacturing).

Placements of all viral injections and implanted fibers were histologically verified (e.g., Figure S5) at the termination of the experiments using DAPI staining of 100-μm coronal sections (ProLong Gold Antifade Mountant with DAPI, Invitrogen). A confocal microscope (FV1000, Olympus) was used for fluorescence imaging.

Calcium imaging and analysis

Animal surgery in preparation for calcium imaging was described previously (Barretto et al., 2015; Lee et al., 2017; Sollars and Hill, 2005). Imaging data were obtained using an Evolve 512 EMCCD camera (Photometrics). All images were acquired at 5 Hz, with 10x magnification. A single field of view was analyzed for each ganglion. Tastants were delivered (5–10 mL per min) using silicon tubing positioned approximately 8 mm inside the oral cavity, dorsal to the tongue. Tastants dissolved in water were delivered for 2 s each in serial order, interspersed with 13 s of artificial saliva or water rinse. Images were acquired during epochs of continuous stimulus presentation. The concentrations of tastants used were: AceK, 30 mM; cycloheximide, 0.1 to 1mM; quinine hydrochloride, 5 mM; NaCl, 60 mM; monopotassium glutamate + inosine monophosphate, 100 mM + 1 mM, respectively; citric acid, 50 mM. Because there are very few umami-responding neurons in the mouse geniculate ganglion (Barretto et al., 2015; Lee et al., 2017), they were not included in the analysis.

Imaging data were analyzed using custom software implemented in MATLAB (MathWorks) as described previously (Lee et al., 2017; Yarmolinsky et al., 2016). In essence, neurons were examined for their tuning to various tastes without pre-selection. To identify neurons, maps of peak activity (maximal pixel intensity over mean pixel intensity) were median filtered, thresholded, and separated by watershed segmentation to create candidate regions of interest representing active neurons, which were reviewed manually to identify ROIs for all active neurons. Fluorescence traces for each region of interest were normalized to neighborhood fluorescence intensity (defined as the average intensity within a two-cell radius distance of each cell, excluding all other defined ROIs) to correct for neuropil signal. Calcium transients were scored as fluorescence excursions of >10-fold above noise (defined as median average deviation; equivalent results were obtained with 5-fold). We also visually scored cells by directly observing the aligned image data displayed as a relative fluorescence movie, as well as the putative cells' fluorescence time series (Barretto et al., 2015). To ensure that signals originated from a single neuron, and not from closely adjacent cells or out-of-focus fluorescence from deeper cell layers, we examined the correlation of pixels in the neighborhood of each ROI for each calcium transient, discarding from analysis any neuron contaminated by outside signals (Barretto et al., 2015; Lee et al., 2017; Yarmolinsky et al., 2016).

Cell isolation and sequencing library construction

The TRC isolation process was as described previously (Lee et al., 2017). Cells were extracted from tongues of Pkd2l1-tdTomato mice. After isolation, cells were fractionated using a fluorescence activated cell sorter (MoFlo Astrios, Beckman Coulter). The tdTomato+ (sour TRCs) and tdTomato− (non-sour TRCs and supporting cells) were sorted (50-100 for cell pools, or single cells)

Please cite this article in press as: Zhang et al., Sour Sensing from the Tongue to the Brain, Cell (2019), https://doi.org/10.1016/j.cell.2019.08.031

into 96-well plates containing cDNA synthesis buffer. The cDNA libraries from TRCs for bulk and single cell sequencing were prepared using the SMART-Seq Ultra Low Input RNA kit (TaKaRa) and the Nextera XT DNA Sample Kit (Illumina) using custom indexed adapters.

To dissociate single ganglion neurons, geniculate ganglia from P2rx3-tdTomato animals were isolated and placed in a micro-dish containing 200μl of collagenase/dispase (Roche) solution (4mg/ml in HBSS) at 37°C for 15min. The collagenase/dispase solution was carefully removed without disturbing the tissue, and 200μl papain (Worthington) solution was added to the dish and incubated at 37°C for 15min. Dissociated ganglion cells were spun down, re-suspended in 500 μl HBSS and placed in a collagen-coated micro-dish. To pick single tdTomato+ ganglion neuron, the cell suspension was monitored with an Olympus IX70 inverted fluorescence microscope through the entire picking process. The single-cell sequencing libraries were prepared using the CEL-Seq method as previously described (Hashimshony et al., 2016; Hashimshony et al., 2012). Briefly, the MessageAmp II aRNA Amplification Kit (Invitrogen) was used to obtain amplified RNA (aRNA); aRNA was fragmented and then purified with RNeasy MinElute Cleanup Kit (QIAGEN); cDNA was prepared using Superscipt II (Invitrogen) and libraries were prepared using TruSeq Small RNA Library Preparation Kit (Illumina). The quality of libraries was assessed by bioanalyzer and quantified using quantitative PCR.

Bulk and single cell RNA-seq analysis

Sequencing of custom constructed libraries was carried out at the New York Genome Center using the illumina HiSeq and NextSeq platforms. Paired-end reads were trimmed and aligned to GRCm38 (mm10) using STAR (Dobin et al., 2013). Only uniquely mapped reads were used for gene quantification. Reads per million (RPM) counts for each gene were computed using HTSeq (Anders et al., 2015). Genes enriched in sour TRCs (Table S1) were selected based on differential expression calculated using DESeq (Anders and Huber, 2010) by comparing gene expression in Pkd2l1-labeled sour cells and control cells.

Single cell RNA-seq clustering and neuronal cluster marker identification was carried out using the Seurat R package (https://satijalab.org/seurat) as previously described (Butler et al., 2018; Satija et al., 2015). Custom R code was generated according to online instructions and vignettes. A total of 800 single geniculate ganglion neurons were sequenced and analyzed. For analysis, 9838 genes from 274 neurons were selected in Seurat based on (a) the gene had to be expressed at >1 RPM and in >3 cells (of the 800), and (b) cells had to show expression of Phox2b at RPM >1, and have more than >2000 genes expressed. The tSNE plots shows 271 (Figure 3; 3 cells were not clustered). Similar clustering results were obtained using all Phox2b-expressing neurons.

Gustometer behavior analysis

Taste behaviors (shown in Figures 4 and 7) were performed using a short-term assay that directly measures taste preference by counting immediate licking responses in a multichannel gustometer (Davis MS160-Mouse gustometer) (Glendinning et al., 2002; Zhang et al., 2003). Mice were acclimated to the gustometer, and trained to lick water from the spouts 2-3 days prior to tests. For attractive tastants (sweet, AceK; umami, monopotassium glutamate + inosine monophosphate), animals were mildly water-deprived for 14 h prior to the tests, and then provided with water trials in the gustometer so they licked no more than 20 licks per 10 s window prior to starting the experiment. To test salt attraction, animals were injected (Intraperitoneal) with furosemide (50mg/kg) 24 h prior to the test and provided with a salt-deficient diet (ENVIGO) (Chandrashekar et al., 2010); water was removed 6-14 h prior to the test. For aversive tastants (sour, citric acid; bitter, quinine), mice were water-deprived for 24 h prior to the tests. All animals were placed individually into the gustometer chamber, and presented with one tastant at a time. Each 10-15 min test session consisted of 10-60 trials. Number of licks, lick latency and inter-lick interval were automatically recorded for each trial.

Fiber photometry

Prior to fiber photometry experiments, an intraoral cannula (used to directly deliver tastants into the animal's oral cavity) was implanted as previously described (Phillips and Norgen, 1970) with the following modifications: the cannula was made of sterile micro-renathane tubing (0.037in diameter, Braintree Scientific) and fitted over a curved needle to facilitate insertion. The needle and cannula was inserted under the skin along the lateral surface of the skull, and exited in the mouth between the cheek and the next to the third maxillary molar. The mouth-end of the cannula was trimmed to extend no more than 2mm into the oral cavity; the loose top end of the cannula was affixed to the skull with dental cement. At least 3 days after surgery, animals were adapted to intraoral infusion by receiving water through the cannula (0.8ml/min, 15 min) using a syringe pump for 3 daily sessions. During photometry recording sessions each infusion trial consisted of a 30 s pre-infusion interval, 10 s of tastant (0.8ml/min), and 30 s post-infusion interval. Water was flowing through the cannula during the pre- and post-infusion intervals (0.8ml/min).

Population-level GCaMP fluorescence was recorded using fiber photometry as described previously (Gunaydin et al., 2014). Briefly, 465nm and 405nm light from light-emitting diodes (Doric Lenses) were combined in a connectorized fluorescence minicube (Doric) and delivered into the brain. The emission fluorescence was focused onto a femtowatt photodetector (NewPort), amplified by Brownlee Precision Model 440 amplifier, and digitized and recorded with LabJack U6-Pro at100Hz sampling rate. The collected data were analyzed using custom MATLAB code. The dF/F ratio was calculated as: $(F-F_0)/F_0$, where F_0 was the median fitted 405 signal in a 3 s time window before the onset of tastant infusion. The calcium transient was identified using validated statistical measures (the median and Qn estimator) (Rousseeuw and Croux, 1993), and the area under the curve (AUC) was calculated by integrating fluorescence signal under identified calcium transients. Traces were smoothed using moving average and down-sampled to 1 Hz.

Retrograde monosynaptic tracing

Monosynaptic tracing experiments were performed as described previously (Reardon et al., 2016; Wickersham et al., 2007a; Wickersham et al., 2007b). The rNST (coordinate: bregma 6.4mm; lateral 1.1mm; ventral 4.0mm) of Pdyn-Cre animals were first injected with 100 nL of 1:1 mixture of AAV1-DIO-TVA-mcherry (UNC vector core) and AAV1-DIO-G(N2C)-mKate (Janelia viral core), followed by a second injection of 100nl rabies virus carrying GFP expression cassette (RABV-ΔG-GFP, Janelia viral core) 3 weeks later. Two weeks after RABV infection, the animals were euthanized for histological examination of *trans*-synaptic transfer. All injections were bilateral.

Fluorescent *in situ* hybridization

Fresh frozen tissues were sectioned (16 μm/section) and processed for mRNA detection using RNAscope (Advanced Cell Diagnostics) according to the manufacturer's protocol. Sections were then imaged using confocal microscope (FV1000, Olympus). The following probes were used: eGFP (Cat# 400288-C2), Penk (Cat# 318761), Cdh13 (Cat# 443251) and Trpv1 (Cat# 313331).

Optogenetic stimulation in lick preference assays

Lick preference with and without light stimulation (Figures 6B, 6C, and S6E) was measured in head-attached animals by using a custom-built gustometer, see above and also described in Peng et al. (2015). Prior to testing, mice were habituated to the behavioral chamber and trained to lick from swing-in spout (Peng et al., 2015). Each testing session (Figures 6B and 6C) was initiated with a light cue, and consisted of 20 trials with water, half of which were randomly coupled to photostimulation. For dry lick tests (Figure S6E), animals were presented with 20 dry trials (half of them were randomly coupled to light). These dry trials were interspersed with 20 water trials to encourage the thirsty animals to lick during dry trials. Licking events were detected by a capacitive touch sensor (MPR121, SparkFun) and registered by a custom-written code in MATLAB via Arduino (Arduino Mega 2560, Arduino). For photostimulation, 473-nm light stimuli (diode-pumped solid-state laser, Shanghai Laser & Optics Century, or fiber-coupled LED, Thorlabs) were delivered via an optical fiber implanted over the rNST. Light stimulation was triggered by contact of the tongue with the metal spout; one lick triggered a train of light pulses (20 Hz, 20 ms per pulse, 20 pulses, 5–15 mW per mm2). Licks during the light stimulation extended the stimulus for 1 s after the last lick. Light cues, the delivery of tastants and positioning of the spout were controlled using a MATLAB program via a microcontroller board (Arduino Mega 2560, Arduino).

Three-port taste-recognition assay

Mice deprived of water for 24 h were trained to perform a taste-recognition task in a customized three-port behavior chamber as described previously (Wang et al., 2018). Taste cues (1mM quinine or 20mM citric acid) were randomly delivered through a metal spout in the middle port. Mice were given (up to) 60 s to initiate a trial by licking the middle spout. If a trial was initiated, mice were allowed to sample tastant cues (2-3 μl) for 2 licks and then given 4 s to make a left or right choice to obtain a water reward (total ~6 μl). For a given mouse, reward from side ports was pre-assigned to taste cues (for example, left for bitter, right for sour). A wrong choice triggered a penalty of a 5 s timeout. Mice were trained for two sessions (80–100 pseudo-randomized trials each) per day until they could effectively discriminate the bitter and sour with >70% accuracy (2–3 weeks). A third cue, water, was then introduced into the training and the animals were rewarded at the same port as the bitter side. Testing sessions consisted of 86 pseudo-randomized trials, with 10 trials of water (rewarded if correct) and 10 trials of water + laser (unrewarded); the other 66 trials were divided between bitter and sour trials (70% rewarded trials and 30% unrewarded trials to hinder conditioning during testing). The licks were detected by a capacitive touch sensor (MPR121, Adafruit). The delivery of tastants, shutter position, and light stimuli were controlled by a custom written program in MATLAB via an Arduino board.

Trigeminal microinjection

Resiniferotoxin (RTX) was prepared and injected into the trigeminal ganglia as previously described (Karai et al., 2004; Mishra and Hoon, 2010). RTX (0.25μg/μl in PBS, 1.5 μl per ganglion) was injected at coordinates: bregma 6.3mm; lateral 1.3mm; ventral 6.3mm.

QUANTIFICATION AND STATISTICAL ANALYSIS

The statistical tests used in this study are indicated in the respective figure legends. In general, data with single independent experiments were analyzed by unpaired t tests to determine statistical significant effects ($p < 0.05$). When several tastant concentrations were used, multiple unpaired t tests were used to calculate significance at each concentration ($p < 0.05$). Data from multiple independent animal groups were analyzed by ANOVA to determine statistical significance ($p < 0.05$).

DATA AND CODE AVAILABILITY

The accession number for the sequence data reported in this paper is GEO: GSE135801.

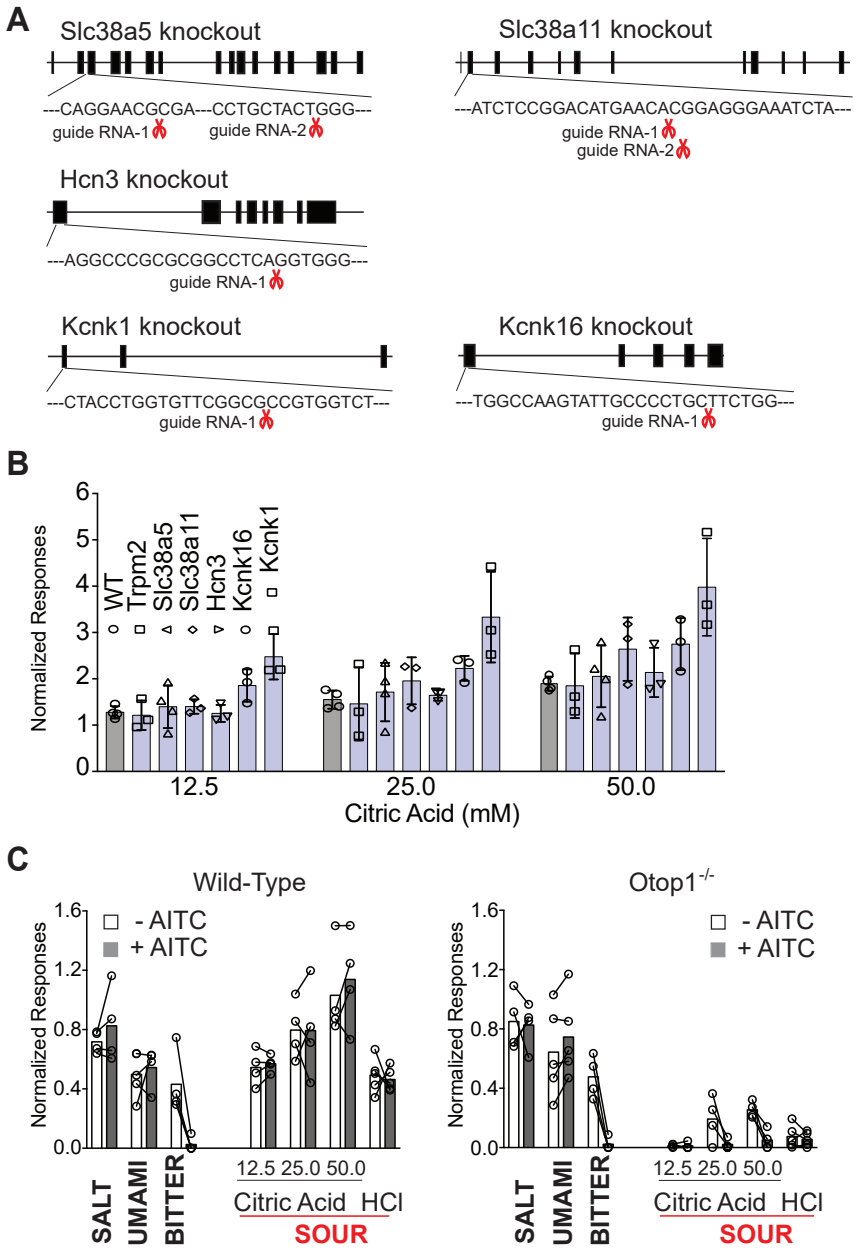

Figure S1. Characterization of Candidate Sour Receptor Knockouts, Related to Figure 1

(A) Schematic drawing illustrating the structure of Slc38a5, Slc38a11, Hcn3, Kcnk1 and Kcnk16, including the strategy used for generating knockouts using CRISPR-Cas9; the method used for generating Otop1 knockouts is described in Figure 1. The sequence of the targeted region is shown under the cartoons; red scissors denote the cutting positions. All knockouts were validated by sequencing the targeted locus in homozygous mutants prior to establishing lines for nerve recordings. The Slc38a5$^{-/-}$ animals carry a 2 bp deletion, resulting in early termination after amino acid residue #39; the Slc38a11$^{-/-}$ animals carry 1 bp deletion, resulting in early termination after amino acid residue #35; Hcn3$^{-/-}$ animals carry a 79 bp deletion, resulting in early termination after amino acid residue #43; Knck1$^{-/-}$ animals carry a 14 bp deletion, resulting in early termination after amino acid residue #43; Kcnk16$^{-/-}$ animals carry a 2 bp insertion, resulting in early termination after amino acid residue #55.

(B) Quantification of nerve responses of WT control (gray bar, n = 4) and homozygous knockout mice for: Trpm2 (n = 3), Slc38a5 (n = 4), Slc38a11 (n = 3), Hcn3 (n = 3), Kcnk16 (n = 3), and Kcnk1 (n = 3). To prevent confounds from genetic differences in the sweet receptor gene in the various strains (i.e., *taster* versus *non-taster*) (Bachmanov et al., 2001), nerve responses were normalized to the responses to 100mM NaCl. Values are means ± s.e.m. (the average of 2 separate recording sessions were used per animal). No significant decrease in nerve responses was observed in these mutants (Knck1$^{-/-}$ and Kcnk16$^{-/-}$ showed significant increase in nerve responses compared with WT animals), multiple t tests.

(C) Quantification of nerve responses from control (left) and Otop1$^{-/-}$ homozygous mutants (right), before (white bars) and after (gray) blocking acid-evoked responses from bitter TRCs with AITC (Barretto et al., 2015; Oka et al., 2013). Otop1$^{-/-}$ mutants were backcrossed to ensure they carry the *taster* allele of the

(legend continued on next page)

sweet gene (Bachmanov et al., 2001). Nerve responses were normalized to the responses to 30mM AceK. Shown are quantified responses to salt (100mM NaCl, n = 4), umami (30mM MPG with 1mM IMP, n = 5), bitter (5mM Quinine, n = 4) and a panel of sour tastants, including Citric Acid (12.5mM, 25mM and 50mM, n = 4) and Hydrochloric Acid (HCl, 10mM, n = 5). Previously, we showed that a subset of bitter TRCs respond to acid stimulus, likely as a result of some T2R GPCRs being sensitive to low pH (Barretto et al., 2015; Oka et al., 2013). These bitter cell-originated acid responses selectively activate bitter ganglion neurons (but not sour), are blocked by silencing bitter TRCs, and are independent of the activity of sour TRCs (i.e., they remain in the total absence of sour TRCs, but are abolished after blocking bitter TRC function) (Barretto et al., 2015; Oka et al., 2013). Therefore, to prevent contamination of signals from bitter TRCs, recordings were carried out in the presence of the bitter cell blocker AITC (Oka et al., 2013). As expected, residual responses to acid stimuli in Otop1$^{-/-}$ animals were abolished after AITC-treatment; these originate from bitter TRCs (Barretto et al., 2015; Oka et al., 2013). There were no significant differences in responses to other tastants before and after AITC. WT versus Otop1$^{-/-}$ before AITC treatment: $p = 0.0008$ (12.5 mM CA), $p = 0.014$ (25 and 50 mM CA) and $p = 0.001$ (10 mM HCl). WT versus Otop1$^{-/-}$ after AITC treatment, $p < 0.01$ for all acids. The sour data presented in this figure comes from Figure 1C.

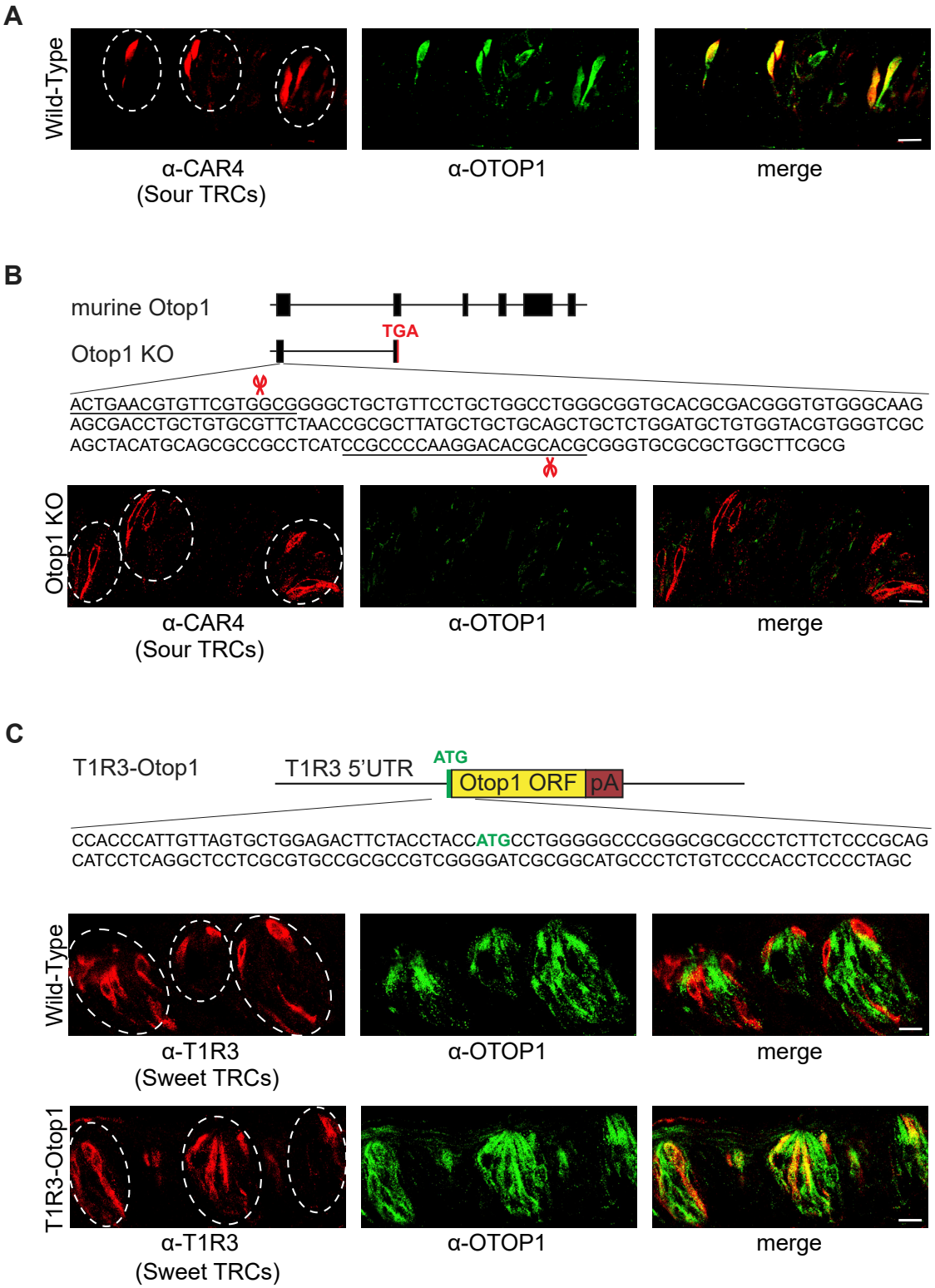

Figure S2. OTOP1 Is Not Expressed in Otop1$^{-/-}$ Mutants, Related to Figures 1 and 2

(A) Sour TRCs were identified by the selective expression of carbonic anhydrase-4 (CAR4) (Chandrashekar et al., 2009). Shown are co-immunofluorescence staining of circumvallate papillae of WT taste buds labeled with anti-CAR4 antibodies to mark sour TRCs (shown in red, left panel) and anti-OTOP1 antibodies

(legend continued on next page)

(shown in green, middle panel). The dotted ovals highlight the position of taste buds; note the expected co-localization of OTOP1 and CAR4 in sour TRCs. Scale bars, 50 μm.

(B) Schematic drawing illustrating the structure of the murine Otop1 gene and the strategy for generating knockouts using CRISPR-Cas9 (expanded from Figure 1). Partial sequence of exon 1 are shown below the diagram to mark the location of the two guide RNA sequences (underlined) and the cutting positions (red scissors). Sanger sequencing of the targeted region verified the 166 bp deletion in exon 1, resulting in early termination in exon 2. The panels below show immunofluorescence staining of OTOP1 in circumvallate papillae of the mutant animals. Note the total loss of OTOP protein in the knockout (middle panel; compare with [A]). Dotted ovals show the location of taste buds. Red, anti-CAR4 antibody staining. Scale bars, 50 μm.

(C) Schematic drawing illustrating the structure of the T1R3-Otop1 knockin locus (top panel). The entire open reading frame of murine Otop1 (Otop1 ORF, including BGH polyA sequences) was inserted immediately following the start codon (ATG) of the T1R3 gene. Bottom panels show immunofluorescence staining of T1R3 (red, left) and Otop1 (green) of taste buds in circumvallate papillae of WT and T1R3-Otop1 animals. Dotted ovals demark taste buds. Scale bars, 50 μm. Note that sweet TRCs (T1R3-expressing) in the T1R3-Otop1 engineered mice now also express Otop1.

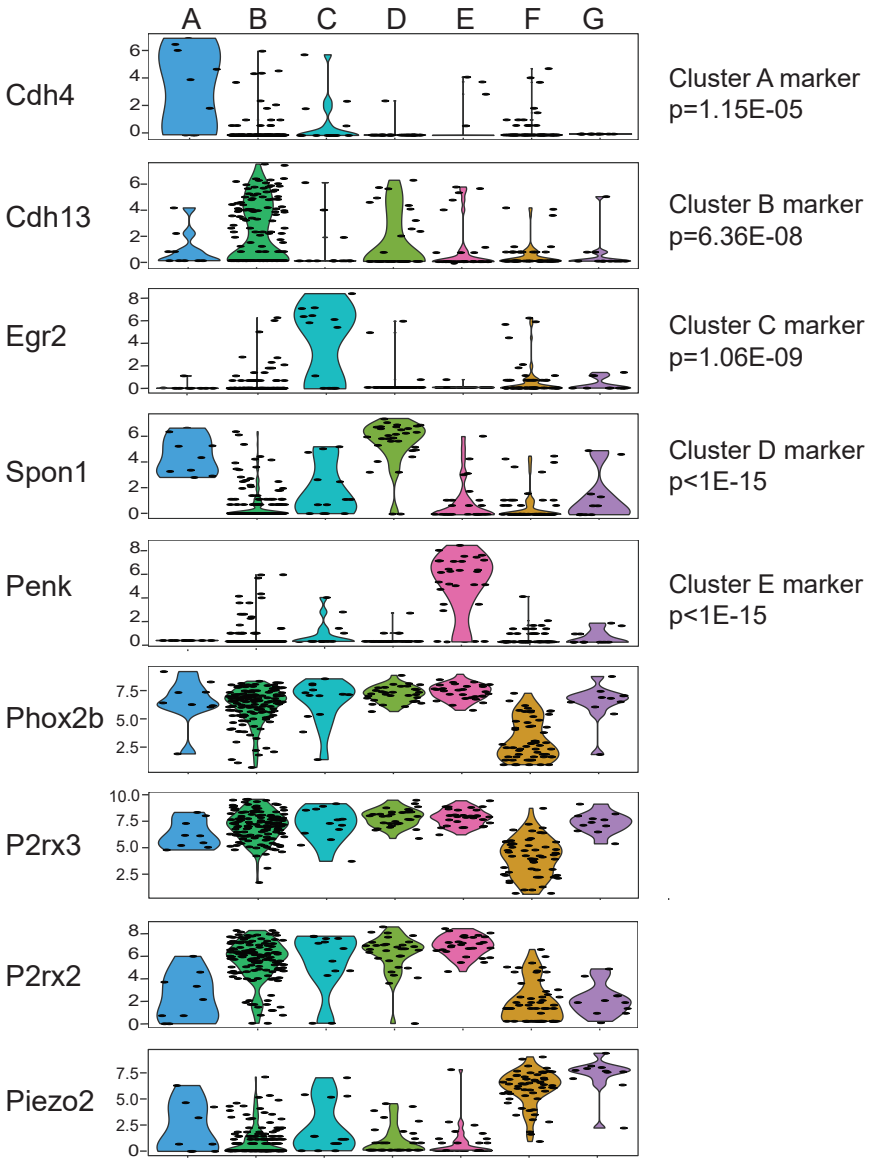

Figure S3. Gene Markers Defining Geniculate Ganglion Clusters, Related to Figure 3

Shown are violin plots for ganglion neuron markers used in this study, generated using Seurat (Butler et al., 2018). Expression levels are shown on the y axis as the ln (transcript per million). p values were calculated in Seurat by comparing a gene's specific distribution to a distribution assuming the gene in question would be uniformly expressed in the population) (Butler et al., 2018).

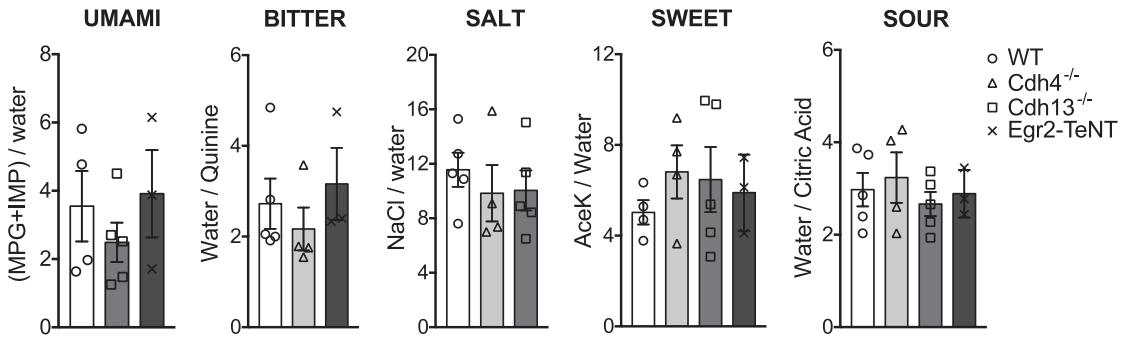

Figure S4. Characterization of Ganglion Neuron Taste Clusters, Related to Figure 4

Quantification of behavioral taste preference assays (Zhang et al., 2003) for WT control (WT, white bars, n = 5) Cdh4$^{-/-}$ mutants (light gray bars, n = 4), Cdh13$^{-/-}$ mutants (gray bars, n = 5) and Egr2-TeNT animals with silenced Egr2 -expressing neurons (dark gray, n = 3). Taste preferences for umami (7.5mM MPG with 1mM IMP), bitter (0.3mM Quinine), Salt (240mM NaCl,), sweet (5mM AceK) and sour (20mM Citric Acid) are shown relative to water. Cdh4$^{-/-}$ animals no longer exhibit preference for umami solutions (Figure 4B), but their behavioral responses to bitter, salt, sweet, sour were not significantly different from WT controls; Cdh13$^{-/-}$ animals have deficits in bitter aversion (Figure 4C), but their responses to umami, salt, sweet, and sour were not significantly different from WT controls; Egr2-TeNT animals exhibited loss of salt attraction (Figure 4D), but their responses to umami, bitter, sweet, and sour were not significantly different from WT controls. Values are means ± s.e.m. For each taste quality, statistical significance was tested using one-way ANOVA.

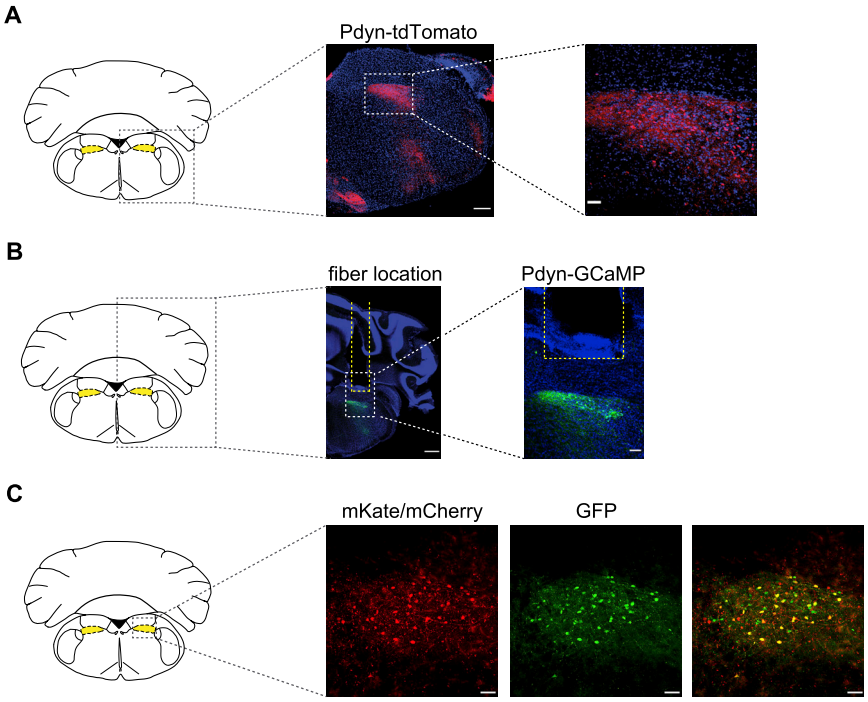

Figure S5. Reporter Expression in Pdyn Neurons and Retrograde Monosynaptic Tracing from the rNST, Related to Figure 5

(A) Diagram of a coronal brain section highlighting the rNST area in yellow (left panel). The right panels show increasing magnifications of tdTomato reporter expression (from a cross to Ai9 reporter animals) (Madisen et al., 2010) in the rostral NST in Pdyn-Cre expressing neurons. Note the enrichment of labeled neurons; middle panel scale bar, 250 μm; right panel scale bar, 50 μm. See The Mouse Brain in Stereotaxic Coordinates for anatomical details (Paxinos and Franklin, 2003).

(B) Diagram of coronal section highlighting the rNST area in yellow (left panel). The right panels show a sample section of an animal used for fiber photometry experiments, highlighting the location of the fiber as traced by the fiber tracks in post hoc histological examinations. The same section also shows the Pdyn neurons in the rNST expressing GCaMP (green label); middle panel scale bar, 500 μm; right panel scale bar, 100 μm. Yellow dashed lines indicate the location of photometry fiber.

(C) Rotrostral NST of Pdyn-Cre animals were bilaterally infected with a mixture of AAV-DIO-TVA-mCherry and AAV-DIO-G(N2C)-mKate, followed by infection with RABV-GFP (Figure 5D). Left panel, diagram of the brain area highlighting the NST (adapted from The Mouse Brain in Stereotaxic Coordinates). The mKate panel shows NST neurons infected by AAV-DIO- G(N2C)-mKate; the GFP panel shown NST neurons infected RABV-ΔG-GFP. The rightmost panel shows the overlap; these are the "starter" cells. Scale bars, 100 μm.

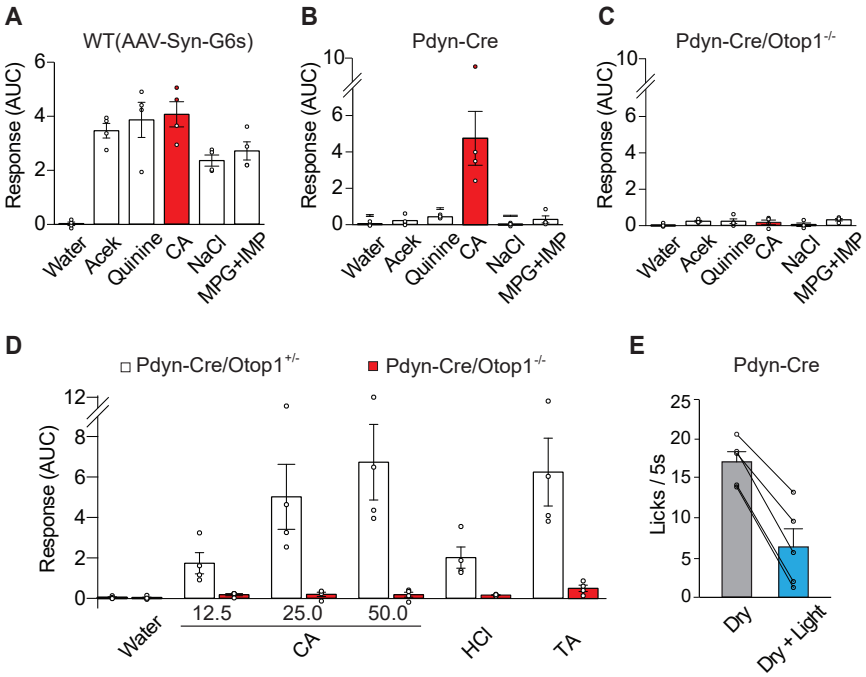

Figure S6. Quantification of Taste-Evoked Activity in Pdyn-Expressing Neurons in the rNST, Related to Figures 5 and 6

(A) Quantification of evoked population activity in the rNST (from Figure 5B, top row) of animals virally expressing Syn-GCaMP6s in response to 20mM Acek, 5mM Quinine, 50mM Citric Acid, 60mM NaCl, 50mM MPG+1mM IMP (n = 4). AUC: Area Under the Curve (see STAR Methods for details).

(B) Quantification of evoked population activity in rNST of Pdyn-Cre animals (from Figure 5B, middle row) virally expressing Syn-DIO-GCaMP6s in response to 20mM Acek, 5mM Quinine, 50mM Citric Acid, 60mM NaCl, 50mM MPG+1mM IMP. n = 4, multiple unpaired t test. $p < 0.05$ for sour (CA) versus all other tastants.

(C) Quantification of taste evoked activity in rNST of Otop1$^{-/-}$; Pdyn-Cre animals (from Figure 5B, bottom row) virally expressing syn-DIO-GCaMP6s in response to 20mM Acek, 5mM Quinine, 50mM Citric Acid, 60mM NaCl, 50mM+1mM MPG+IMP (n = 4).

(D) Quantification of taste evoked activity in rNST of Otop1$^{-/-}$; Pdyn-Cre animals virally expressing Syn-DIO-GCaMP6s in response to a panel of sour tastes (12.5, 25, 50mM CA, 10mM HCl and 50mM TA, n = 4, multiple unpaired t test, $p < 0.05$ for all columns)

(E) To determine whether ingestion is required for the light-dependent suppression of licking (see Figure 6B), we performed similar experiments under conditions where the spout delivered no water in the trial before and during the light stimulation (see Methods for details). Shown is the quantitation of dry licking responses with and without light stimulation of Pdyn-expressing neurons in rNST (n = 5, paired t test, $p < 0.001$). These results demonstrate that ingestion is not necessary for lick suppression.

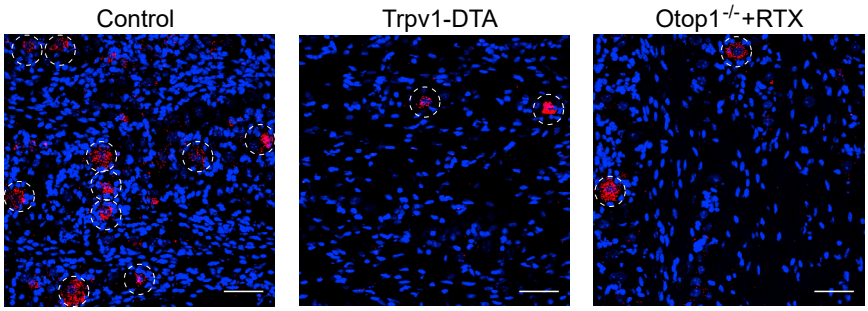

Figure S7. Ablation of Trpv1-Expressing Trigeminal Neurons, Related to Figure 7

RNA FISH of Trpv1 (red) in control (WT, left panel), Trpv1-DTA (middle panel), and Otop1$^{-/-}$ animals injected with RTX (right panel). RTX injection and diphtheria toxin ablated >70% of Trpv1-expressing neurons. Scale bars, 50 μm.